

The ErbB4 CYT2 variant protects EGFR from ligand-induced degradation to enhance cancer cell motility

Tai Kiuchi, Elena Ortiz-Zapater, James Monypenny, Daniel R. Matthews, Lan K. Nguyen, Jody Barbeau, Oana Coban, Katherine Lawler, Brian Burford, Daniel J. Rolfe, Emanuele de Rinaldis, Dimitra Dafou, Michael A. Simpson, Natalie Woodman, Sarah Pinder, Cheryl E. Gillett, Viviane Devauges, Simon P. Poland, Gilbert Fruhwirth, Pierfrancesco Marra, Ykelien L. Boersma, Andreas Plückthun, William J. Gullick, Yosef Yarden, George Santis, Martyn Winn, Boris N. Kholodenko, Marisa L. Martin-Fernandez, Peter Parker, Andrew Tutt, Simon M. Ameer-Beg and Tony Ng (August 19, 2014)
Science Signaling 7 (339), ra78. [doi: 10.1126/scisignal.2005157]

The following resources related to this article are available online at <http://stke.sciencemag.org>.
This information is current as of August 19, 2014.

Article Tools	Visit the online version of this article to access the personalization and article tools: http://stke.sciencemag.org/content/7/339/ra78
Supplemental Materials	" <i>Supplementary Materials</i> " http://stke.sciencemag.org/content/suppl/2014/08/15/7.339.ra78.DC1.html
Related Content	The editors suggest related resources on <i>Science's</i> sites: http://stke.sciencemag.org/content/sigtrans/6/287/ra66.full.html http://stke.sciencemag.org/content/sigtrans/7/318/ra29.full.html http://stke.sciencemag.org/content/sigtrans/2/102/ra86.full.html
References	This article cites 88 articles, 47 of which you can access for free at: http://stke.sciencemag.org/content/7/339/ra78#BIBL
Glossary	Look up definitions for abbreviations and terms found in this article: http://stke.sciencemag.org/cgi/glossarylookup
Permissions	Obtain information about reproducing this article: http://www.sciencemag.org/about/permissions.dtl

Science Signaling (ISSN 1937-9145) is published weekly, except the last December, by the American Association for the Advancement of Science, 1200 New York Avenue, NW, Washington, DC 20005. Copyright 2014 by the American Association for the Advancement of Science; all rights reserved.

The ErbB4 CYT2 variant protects EGFR from ligand-induced degradation to enhance cancer cell motility

Tai Kiuchi,^{1,2,3,*†} Elena Ortiz-Zapater,^{4*} James Monypenny,^{1,2,3*} Daniel R. Matthews,^{1,2‡} Lan K. Nguyen,⁵ Jody Barbeau,^{1,2} Oana Coban,^{1,2} Katherine Lawler,^{1,2} Brian Burford,³ Daniel J. Rolfe,⁶ Emanuele de Rinaldis,³ Dimitra Dafou,⁷ Michael A. Simpson,⁷ Natalie Woodman,^{8,9} Sarah Pinder,^{8,9} Cheryl E. Gillett,^{8,9} Viviane Devauges,^{1,2} Simon P. Poland,^{1,2} Gilbert Fruhwirth,^{1,2§} Pierfrancesco Marra,³ Ykelien L. Boersma,^{10¶} Andreas Plückthun,¹⁰ William J. Gullick,¹¹ Yosef Yarden,¹² George Santis,⁴ Martyn Winn,¹³ Boris N. Kholodenko,⁵ Marisa L. Martin-Fernandez,⁶ Peter Parker,^{2,14} Andrew Tutt,³ Simon M. Ameer-Beg,^{1,2||} Tony Ng^{1,2,3,15||}

The epidermal growth factor receptor (EGFR) is a member of the ErbB family that can promote the migration and proliferation of breast cancer cells. Therapies that target EGFR can promote the dimerization of EGFR with other ErbB receptors, which is associated with the development of drug resistance. Understanding how interactions among ErbB receptors alter EGFR biology could provide avenues for improving cancer therapy. We found that EGFR interacted directly with the CYT1 and CYT2 variants of ErbB4 and the membrane-anchored intracellular domain (mICD). The CYT2 variant, but not the CYT1 variant, protected EGFR from ligand-induced degradation by competing with EGFR for binding to a complex containing the E3 ubiquitin ligase c-Cbl and the adaptor Grb2. Cultured breast cancer cells overexpressing both EGFR and ErbB4 CYT2 mICD exhibited increased migration. With molecular modeling, we identified residues involved in stabilizing the EGFR dimer. Mutation of these residues in the dimer interface destabilized the complex in cells and abrogated growth factor-stimulated cell migration. An exon array analysis of 155 breast tumors revealed that the relative mRNA abundance of the ErbB4 CYT2 variant was increased in ER⁺ HER2⁻ breast cancer patients, suggesting that our findings could be clinically relevant. We propose a mechanism whereby competition for binding to c-Cbl in an ErbB signaling heterodimer promotes migration in response to a growth factor gradient.

INTRODUCTION

The ErbB tyrosine kinase receptor family comprises four members: EGFR [epidermal growth factor receptor; also known as ErbB1 or HER1 (human epidermal growth factor receptor 1)], ErbB2 (HER2), ErbB3 (HER3), and ErbB4 (HER4). At a systems biology level, this receptor signaling network has been described to have a bow-tie architecture (1), which integrates diverse sources of input from the diverse receptor homo- and heterodimers that form in response to EGF and EGF-like growth factor stimulation (2), and channels the resulting signal into several biological outputs through different activation-dependent control loops.

Although the complex ErbB signaling pathways have been therapeutically targeted, the translation of our fundamental biological knowledge into clinically applicable assays for predicting drug response and/or resistance has met considerable challenges that limit the overall therapeutic efficacy (3–6). In breast cancers, detection of increased abundance of EGFR or HER2 by immunostaining does not completely predict clinical outcome of EGFR or HER2-targeted treatments (7, 8). On the other hand, both clinical and preclinical studies have suggested that there is a subpopulation (around a quarter) of EGFR or HER2 normal (not amplified; sometimes labeled as negative) breast cancers that will benefit from these receptor-targeted agents (9, 10). Additional biological mechanisms that may influence the response to EGFR or HER2 targeting treatments therefore need to be elucidated.

Previous studies have shown that cell proliferation and tumorigenesis are enhanced in tumor xenografts coexpressing EGFR with HER2, EGFR with ErbB4, and HER2 with ErbB4 compared to those expressing single ErbB receptors (11–14). These data indicate that in addition to the well-characterized EGFR:HER2 complex, EGFR:ErbB4 could potentially

¹Richard Dimbleby Department of Cancer Research, Randall Division of Cell and Molecular Biophysics, King's College London, Guy's Medical School Campus, London SE1 1UL, UK. ²Division of Cancer Studies, King's College London, London SE1 1UL, UK. ³Breakthrough Breast Cancer Research Unit, Research Oncology, King's College London, Guy's Hospital, London SE1 9RT, UK. ⁴Department of Asthma, Allergy and Respiratory Science, King's College London, Guy's Hospital, London SE1 9RT, UK. ⁵Systems Biology Ireland, University College Dublin, Belfield, Dublin 4, Ireland. ⁶Central Laser Facility, Rutherford Appleton Laboratory, Science and Technology Facilities Council, Research Complex at Harwell, Didcot OX11 0QX, UK. ⁷Genetics and Molecular Medicine, King's College London, Guy's Hospital, London SE1 9RT, UK. ⁸Guy's and St Thomas' Breast Tissue and Data Bank, King's College London, Guy's Hospital, London SE1 9RT, UK. ⁹Research Oncology, Division of Cancer Studies, King's College London, Guy's Hospital, London SE1 9RT, UK. ¹⁰Department of Biochemistry, University of Zurich, 190, 8057 Zurich, Switzerland. ¹¹Department of Biosciences, University of Kent, Canterbury, Kent CT2 7NJ, UK. ¹²Department of Biological Regulation, The Weizmann Institute of Science, Rehovot 76100, Israel. ¹³Computational Science and Engineering Department, Daresbury Laboratory, Science and Technology Facilities Council, Research Complex at Warrington, Warrington WA4 4AD, UK. ¹⁴Protein Phosphorylation Laboratory, Cancer Research UK, London Research Institute, Lincoln's Inn Fields, London WC2A 3PX, UK. ¹⁵UCL Cancer Institute, Paul O'Gorman Building, University College London, London WC1E 6BT, UK.

*These authors contributed equally to this work.

†Present address: Laboratory of Single-Molecule Cell Biology, Tohoku University, Graduate School of Life Sciences, Aoba-ku, Sendai, Miyagi 980-8578, Japan.

‡Present address: The Queensland Brain Institute, The University of Queensland, QBI Building (#79), St Lucia, Queensland 4072, Australia.

§Present address: Department of Imaging Chemistry and Biology Division of Imaging Sciences and Biomedical Engineering School of Medicine King's College London, The Rayne Institute/St. Thomas' Hospital, Lambeth Wing, 4th Floor, London SE1 7EH, UK.

¶Present address: Department of Pharmaceutical Biology, Groningen Research Institute of Pharmacy, A. Deusinglaan 1, 9713 AV Groningen, the Netherlands.

||Corresponding author. E-mail: simon.ameer-beg@kcl.ac.uk (S.A.-B.); tony.ng@kcl.ac.uk (T.N.)

be another important heterodimer that influences the efficacy of EGFR-targeted therapy, although the physical existence of such a dimer has not so far been demonstrated.

In addition to dimer formation, EGFR signaling is also regulated through endocytosis of ubiquitinated receptor cargo, which then undergoes lysosomal degradation (15, 16). A refinement of this mechanism led to the observation of a switch-like behavior, which refers to the sharp increase in ubiquitination followed by subsequent degradation of receptors in cells treated with a ligand concentration above a certain threshold amount that is preset in cells (17). EGF-enhanced EGFR ubiquitination is mediated by the E3 ubiquitin ligase c-Cbl (18), and there is a corresponding threshold-controlled increase in the interaction between EGFR and Cbl [but not with the adaptor proteins Grb2 or Shc (17)]. Furthermore, Grb2 is required for generating the ubiquitinated EGFR threshold. Regulation of the efficient recruitment of the Cbl:Grb2 complex to EGFR is therefore a key node for the activation of ubiquitination and degradation of EGFR and its signal termination.

Our previous work on basal-like breast cancer patient tissues using fluorescence lifetime imaging microscopy (FLIM) histology techniques shows that resistance to EGFR therapy is linked to an increase in EGFR:ErbB3 dimer formation upon treatment (19). Here, we now demonstrate the existence of the EGFR:ErbB4 dimer in breast cancer cells using Förster resonance energy transfer (FRET) measured by FLIM. Using single-particle tracking (SPT) techniques, we measured the rate of change of the in situ concentration of this ErbB heterodimer in response to growth factor stimulation. Moreover, we provide evidence that ErbB4 (as the EGFR:ErbB4 JMa CYT2 protein complex) suppressed ligand-induced EGFR downregulation by sequestering the Cbl:Grb2 component from EGFR. We also identified a differential increase in the relative abundance of the ErbB4 JMa CYT2 splice variant in tumors derived from estrogen receptor–positive (ER⁺) HER2⁻ breast cancer patients [relative to other intrinsic breast cancer subtypes (20)]. ErbB4 JMa CYT2 promoted cell migration in response to soluble ErbB ligands by maintaining a higher steady-state concentration of EGFR for sensing extracellular signals in tumor cells, thus suggesting the pathophysiological importance of this finding. Finally, we showed that dimerization-incompetent EGFR mutants dissociated more rapidly from ErbB4, and the proportion of these EGFR mutants that interacted with ErbB4 was reduced. These mutants were defective in promoting migration in response to growth factor, lending further credence to the promigratory role of this EGFR:ErbB4 heterodimer.

RESULTS

Imaging and biochemical analyses of EGFR heterodimerization with ErbB4 isoforms

The human *ERBB4* gene encodes four alternative splice variants comprising differing extracellular juxtamembrane (JMa and JMb) and cytoplasmic (CYT1 and CYT2) domains (21). The CYT1 isoform has a different cytoplasmic tail from the CYT2 isoform, which contains an additional 16–amino acid stretch that encompasses binding sites for phosphoinositide 3-kinase (22, 23) and for WW domain–containing proteins such as Nedd-like ubiquitin ligases (24–27). JMa is the predominant variant in human breast cancers, with both the CYT1 and CYT2 splice variants present in tumor samples (28). Given the differing biochemical properties of these isoforms, we sought to investigate the spatial distribution of the EGFR:ErbB4 complex in situ. We coexpressed EGFR-enhanced green fluorescent protein (EGFP) with full-length ErbB4-HA [JMa CYT1 or JMa CYT2; stained with anti-hemagglutinin (HA) immunoglobulin G (IgG) conjugated to Cy3] in MCF-7 breast carcinoma cells and determined receptor interactions by

FRET. FRET was monitored using FLIM, which can typically measure protein proximity within the <10-nm range (29–37). Fluorescence lifetime imaging showed that the EGFR-EGFP lifetime values were decreased by ErbB4 coexpression and staining with the acceptor fluorophore-labeled anti-HA IgG, indicating that FRET occurred. The mean FRET efficiency was higher in ErbB4 CYT2 coexpressing cells than in ErbB4 CYT1 coexpressing cells, an effect that was independent of exogenously added EGF (Fig. 1A). Additionally, ErbB4 CYT2 variant–expressing cells had low lifetime (namely, high FRET efficiency) pixels at their periphery, corresponding to an increase in EGFR–ErbB4 CYT2 interaction at the plasma membrane. Unlike EGF, which did not modulate the EGFR–ErbB4 CYT2 association, heparin-binding EGF-like growth factor (HB-EGF), a ligand that binds to both EGFR and ErbB4 (38), caused the dissociation of the EGFR:ErbB4 CYT2 complex (Fig. 1B). Colocalization experiments confirmed that tagged ErbB4 isoforms demonstrated the same pattern of localization as their corresponding untagged forms (fig. S1).

Immunoprecipitation analysis revealed that ectopically expressed EGFR bound not only to full-length ErbB4 CYT1 and CYT2 but also to the membrane-anchored intracellular domain (mICD) of ErbB4 CYT2 (39), as previously reported (40), in the presence or absence of EGF stimulation (Fig. 1C). The lower amount of detectable ErbB4 CYT1 mICD is likely due to the rapid degradation of this truncated form (27, 41). The amount of full-length ErbB4 CYT1 immunoprecipitated with EGFR was less than that observed for either full-length ErbB4 CYT2 or ErbB4 CYT2 mICD (Fig. 1C). Whereas the absence of a baseline reference (nonspecific IgG for instance) makes it difficult to unequivocally confirm the EGFR:ErbB4 CYT1 association in this experiment, these biochemical data further support the observations from our FLIM/FRET (Fig. 1A) studies that demonstrate a constitutive association between these two receptors before and after EGF stimulation. These results suggest that the EGFR:ErbB4 heterodimers in MCF-7 cells are predominantly composed of EGFR and either full-length ErbB4 CYT1, full-length ErbB4 CYT2, or ErbB4 CYT2 mICD. The differing stoichiometry of the interaction between EGFR and the ErbB4 CYT1 and CYT2 isoforms likely explains why the FRET efficiency was higher in cells coexpressing EGFR and ErbB4 CYT2 than in those coexpressing EGFR and ErbB4 CYT1. For the ErbB4 CYT2 isoform, there is a higher acceptor fluorophore-labeled ErbB4 (both full-length and mICD)/EGFR-GFP ratio, whereas for the ErbB4 CYT1 isoform, there is less ErbB4 CYT1 mICD available for labeling with acceptor fluorophore because of degradation. Immunoprecipitation studies confirmed the existence of an endogenous EGFR:ErbB4 heterodimer in T47D cells, which are ER⁺ HER2⁻ breast cancer cells (Fig. 1D).

To determine the functional importance of EGFR:ErbB4 CYT1 and EGFR:ErbB4 CYT2 receptor pairing, we next examined the effects of these heterodimers on EGF-dependent EGFR degradation. In MCF-7 cells coexpressing EGFR and either one of the full-length CYT1 or CYT2 ErbB4 isoforms, expression of the CYT2 isoform of ErbB4, but not CYT1, attenuated EGF-induced degradation of EGFR (Fig. 1E). Therefore, our data suggest that ErbB4 JMa CYT2 is the major ErbB4 isoform that contributes to EGFR:ErbB4 heterodimerization in MCF-7 cells and that this heterodimer confers protection against EGF-dependent EGFR degradation.

Determination of the EGFR:ErbB4 CYT2 dissociation constant by single-molecule imaging

Given the protective effect conferred specifically by the ErbB4 CYT2 isoform on EGFR, we sought to examine in greater detail the signaling and molecular properties of this ErbB4 isoform within the context of EGFR signaling. FRET imaging can be used to spatially map the proportion of interacting and noninteracting components within a cell. When FRET is combined with single-molecule imaging techniques, which enable an in situ

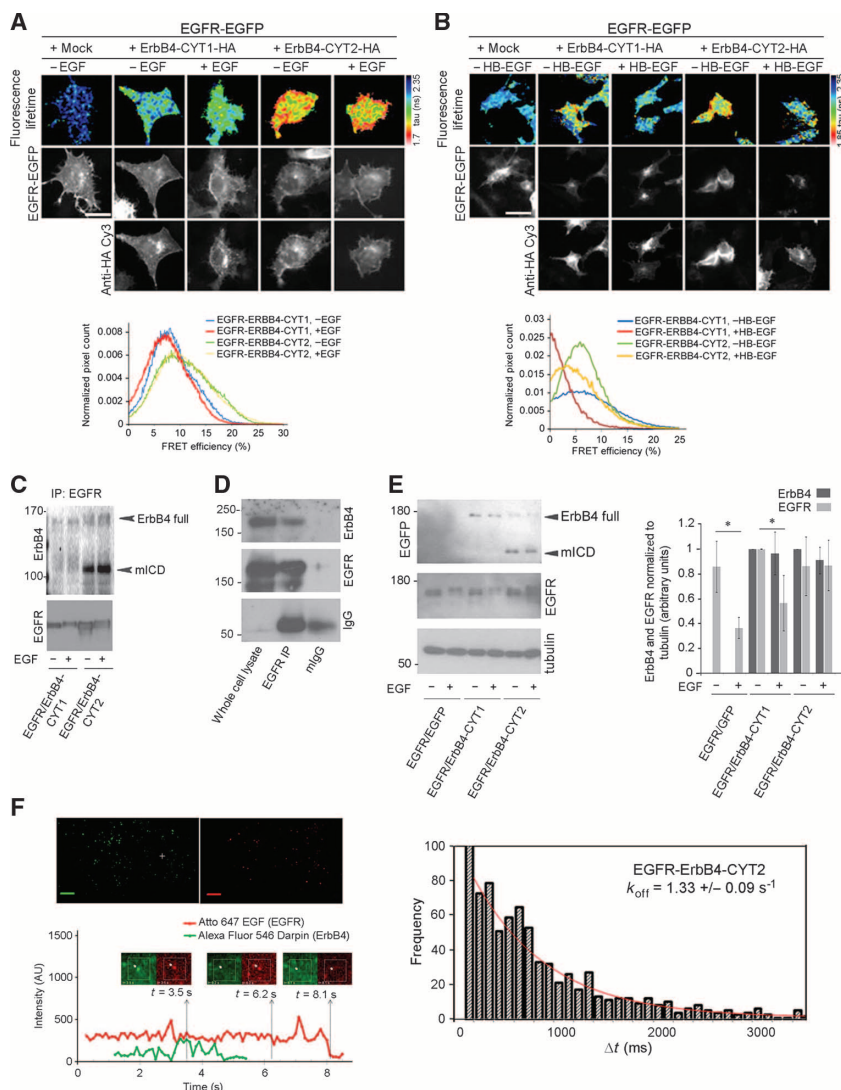


Fig. 1. Analysis of the interaction between EGFR and ErbB4 isoforms by immunoprecipitation and FLIM/FRET combined with live cell SPT. (A) Spatial distribution of EGFR and ErbB4 splice variant heterodimers using FLIM-based FRET measurements. MCF-7 cells expressing EGFR-EGFP plus empty vector or HA-tagged ErbB4 CYT1 or CYT2 variant were stimulated with EGF and stained with anti-HA conjugated to Cy3. Scale bar, 20 μ m. Lifetime images are presented in a blue-to-red pseudocolor scale, with red indicating short lifetime. Bottom: FRET efficiency histograms. Data are means of 10 (EGFR-EGFP alone) or 15 to 21 (EGFR-EGFP and ErbB4-HA with or without EGF) cells ($n = 3$ independent experiments). (B) MCF-7 cells expressing EGFR-EGFP plus empty vector or HA-tagged ErbB4 CYT1 variant or CYT2 variant were stimulated with HB-EGF and stained with anti-HA conjugated to Cy3. Scale bar, 20 μ m. Bottom: FRET efficiency histograms. Data are means of 15 (EGFR-EGFP alone) or 12 to 16 (EGFR-EGFP and ErbB4-HA with or without HB-EGF) cells ($n = 3$ independent experiments). (C) Coimmunoprecipitation analysis of heterodimerization between EGFR and ErbB4 splice variants in MCF-7 cells stimulated or not with EGF (representative blot from three independent experiments). (D) Coimmunoprecipitation of endogenous ErbB4 with endogenous EGFR in T47D cells (representative blot from three independent experiments). (E) Western blot analysis of EGF-dependent degradation of EGFR in MCF-7 cells expressing EGFR plus empty EGFP vector or EGFP-tagged fusions of the ErbB4 CYT1 or CYT2 isoform. Quantification of expression for both EGFR and ErbB4 normalized to tubulin is shown ($n = 3$ independent experiments, $*P < 0.05$). (F) Single-molecule imaging to determine the dissociation constant of the EGFR:ErbB4 complex. MCF-7 cells expressing EGFR and ErbB4 CYT2 were incubated live with EGF-Atto 647N and anti-ErbB4 DARPin conjugated to Alexa 546 (scale bar, 10 μ m). The graph shows the distribution of EGFR:ErbB4 CYT2 heterodimer lifetimes in cells for all accumulated data ($n = 2$ independent experiments per experimental group; the distribution of more than 2000 dimerization events was fitted to a monoexponential).

analysis of the stability of the interaction between individual components, insights into protein-protein associations can be gained because both the stoichiometry (namely, proportion of ErbB4 molecules interacting with EGFR) and the stability of a molecular interaction can be evaluated together. To this end, we next performed single-molecule imaging to determine the rate of change of the concentration of the EGFR:ErbB4 CYT2 heterodimer in situ in response to EGF stimulation. For live cell imaging, we labeled the extracellular sites of these receptors using Atto 647-labeled EGF and an Alexa 546-labeled anti-ErbB4 DARPin (designed ankyrin repeat protein, an antibody-like monovalent molecule with an affinity of 100 pM for ErbB4) (42). By creating a histogram of coincidence times for single molecules of EGF-Atto 647 or DARPin-Alexa 546, we could fit a single exponential decay and determine the k_{off} for EGFR and ErbB4 CYT2 as a measure of the stability of the dimer. The k_{off} for the interaction between wild-type EGFR and full-length ErbB4 CYT2 was $1.33 \pm 0.09 \text{ s}^{-1}$ (Fig. 1F).

Differential increase in the expression of the *ERBB4* CYT2 splice variant in ER⁺ HER2⁻ breast tumors according to exon array analysis

To examine the relative abundance of the ErbB4 JMa CYT1 and CYT2 variants in breast cancer tumor samples, we used exon array analysis. The relative contribution of each variant to the total *ERBB4* expression in a tumor sample can be discerned from the relative abundance of this *CYT1*-specific exon (Fig. 2A, green box) in comparison to the abundance of other exons shared by both variants. The absolute expression of the *CYT1* variant was relatively constant between tumor samples irrespective of ER and HER2 status [Fig. 2, A (green box) and B (lower panel)], indicating that the variations in total *ERBB4* expression between tumor subtypes were due to differences in the expression of the *CYT2* variant (Fig. 2C). Therefore, we concluded from our analysis of 155 tumors from breast cancer patients that there was a differential increase in the relative expression of the *ERBB4* *CYT2* variant specifically among ER⁺ HER2⁻ patients, which highlights the relevance of the EGFR:ErbB4 CYT2 heterodimer in breast tumors. In addition, we analyzed a set of RNA sequencing data from 404 cases of ER⁺ breast cancer patients. Comparison of median total

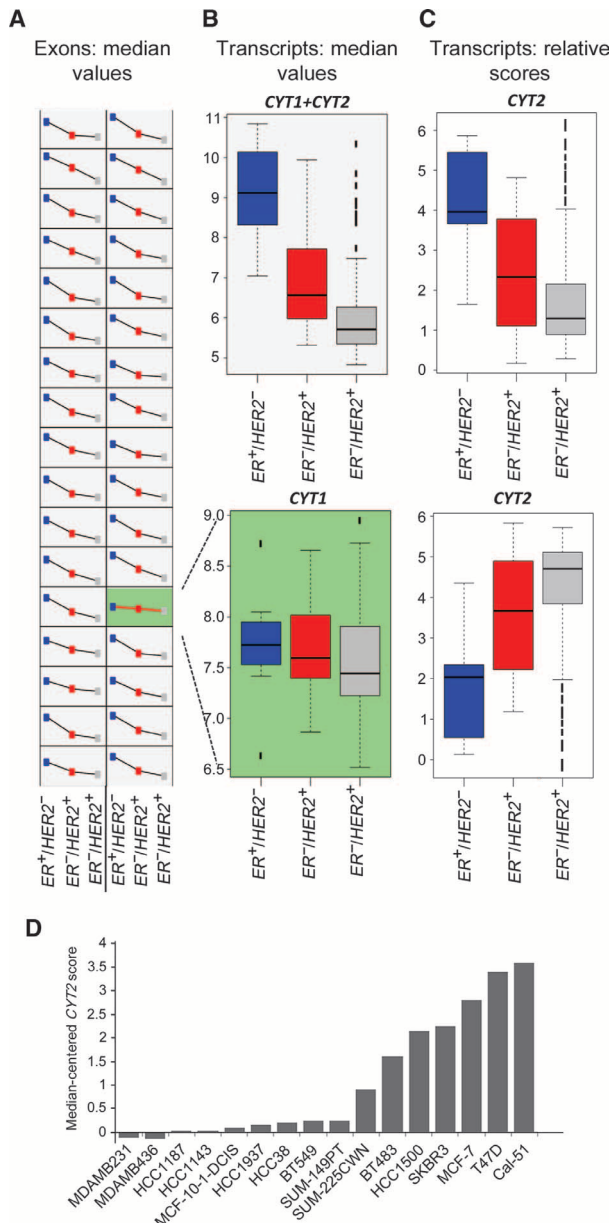


Fig. 2. Transcript abundance of ErbB4 and its variants in human breast cancer samples and in breast cancer cell lines. Transcript abundance of ErbB4 variants, grouped according to immunostaining signals for ER and HER2. ER⁺HER2⁻, $n = 16$ breast tumor samples; ER⁺HER2⁺, $n = 19$ samples; ER⁻HER2⁺, $n = 120$ samples. (A) Trends for the median intensity values of individual exons across the three cancer groups. Each box shows the expression of an ErbB4 exon-related probe set and displays the trend across the three tumor types. The probe set referring to the CYT1-specific exon is highlighted (green box). (B) Top: median intensity values of combined CYT1/2 variants, as inferred from the analysis of common exons. Bottom: median intensity values of CYT1, as inferred from the analysis of the CYT1-specific exon. (C) Relative scores for the CYT1 and CYT2 variants, indicating the relative contribution of CYT2 (top) and CYT1 (bottom) to overall ErbB4 transcript abundance across the three cancer groups. (D) Summary of the median-centered ErbB4 CYT2 score across a panel of different breast cancer cell lines. The CYT2 score is measured as the difference between transcript abundance and CYT1-specific exon expression.

(CYT1 + CYT2) expression and median CYT1 expression showed that there is an overall increase in relative CYT2 expression in the ER⁺HER2⁻ samples (fig. S2), consistent with our exon array-based analysis of 155 tumors.

We carried out a similar *ERBB4* exon array analysis for 16 breast cancer cell lines. Most of the cell lines had high expression of the *ERBB4* CYT2 variant (Fig. 2D), including the T47D cell line, which we used for EGFR: ErbB4 coimmunoprecipitation assays (Fig. 1D).

Functional importance of the endogenous EGFR:ErbB4 CYT2 heterodimer

We next determined the effects of endogenous ErbB4 knockdown on the stability of exogenously expressed EGFR in MCF-7 cells (because the abundance of EGFR in these cells is low). After EGF stimulation, the amount of exogenously expressed EGFR was reduced in MCF-7 cells with ErbB4 knockdown compared to control cells (Fig. 3A). To check that this protective effect on EGFR was ErbB4-specific, we performed the same experiment using cell lines in which ErbB2, ErbB3, or ErbB4 had been stably knocked down (fig. S3). We found that only ErbB4 knockdown produced an EGF-dependent reduction in the amount of EGFR (Fig. 3B). In ErbB4 knockdown cells, EGFR ubiquitination (which is required for EGFR degradation) was increased both before and after EGF stimulation, compared to control cells (Fig. 3C). The recruitment of c-Cbl to EGFR was increased in both the resting state and after ligand stimulation in ErbB4 knockdown cells (Fig. 3C). Therefore, these results suggest that ErbB4, specifically the CYT2 variant, inhibits EGFR ubiquitination and degradation by suppressing c-Cbl binding to EGFR.

Molecular characterization of the binding of c-Cbl to ErbB4 CYT2 mICD

To further investigate the molecular mechanism underlying the effect of the EGFR:ErbB4 heterodimer on the down-regulation of EGFR, we analyzed whether the ErbB4 splice variants differentially associated with endogenous c-Cbl before and after EGF stimulation. Coimmunoprecipitation assays showed that c-Cbl bound to the ErbB4 CYT2 variant but not the CYT1 variant before and after EGF stimulation (Fig. 3D).

Because regulation of the efficient recruitment of the c-Cbl:Grb2 complex to EGFR is a key node for activating the threshold-controlled ubiquitination and clathrin-independent endocytosis of EGFR (17), we sought to identify the region of the ErbB4 intracellular domain that competes with EGFR for c-Cbl binding within the EGFR:ErbB4 dimer. From a sequence homology search comparing ErbB4 with EGFR, we identified a putative direct c-Cbl binding site (Tyr¹¹²⁴) and several potential indirect Cbl sites (through Grb2 binding; Tyr¹¹⁸⁸, Tyr¹²⁰², and Tyr¹²⁴²) within the intracellular domain of ErbB4 (43). We constructed a series of C-terminal truncation mutants of EGFP-tagged ErbB4 mICD that terminated at the residue N-terminal to each of these potential c-Cbl-binding tyrosine residues (fig. S4). Coimmunoprecipitation assays indicated that c-Cbl bound to both wild-type and $\Delta 1242$ ErbB4 CYT2 mICD, but not the $\Delta 1188$, $\Delta 1124$, and $\Delta 1202$ truncation mutants (Fig. 3E), indicating that the major c-Cbl binding site(s) lies within the C-terminal region of the intracellular domain between residues 1202 and 1242. Loss of c-Cbl binding correlated with a reduction of Grb2 binding to ErbB4 CYT2 mICD (Fig. 3E), indicating that c-Cbl recruitment is probably indirect and mediated by the Grb2 adaptor. Finally, we wanted to see the importance of this c-Cbl interaction in the ErbB4 CYT2 mICD-dependent protection of EGFR after ligand binding. Western blot analysis revealed that, unlike ErbB4 CYT2 mICD, which binds to c-Cbl, the ErbB4 CYT2 mICD $\Delta 1202$ mutant did not protect exogenously expressed EGFR from degradation after EGF stimulation (Fig. 3F). Expression of ErbB4 CYT2 mICD protected EGFR from degradation after treatment with EGF but not with HB-EGF.

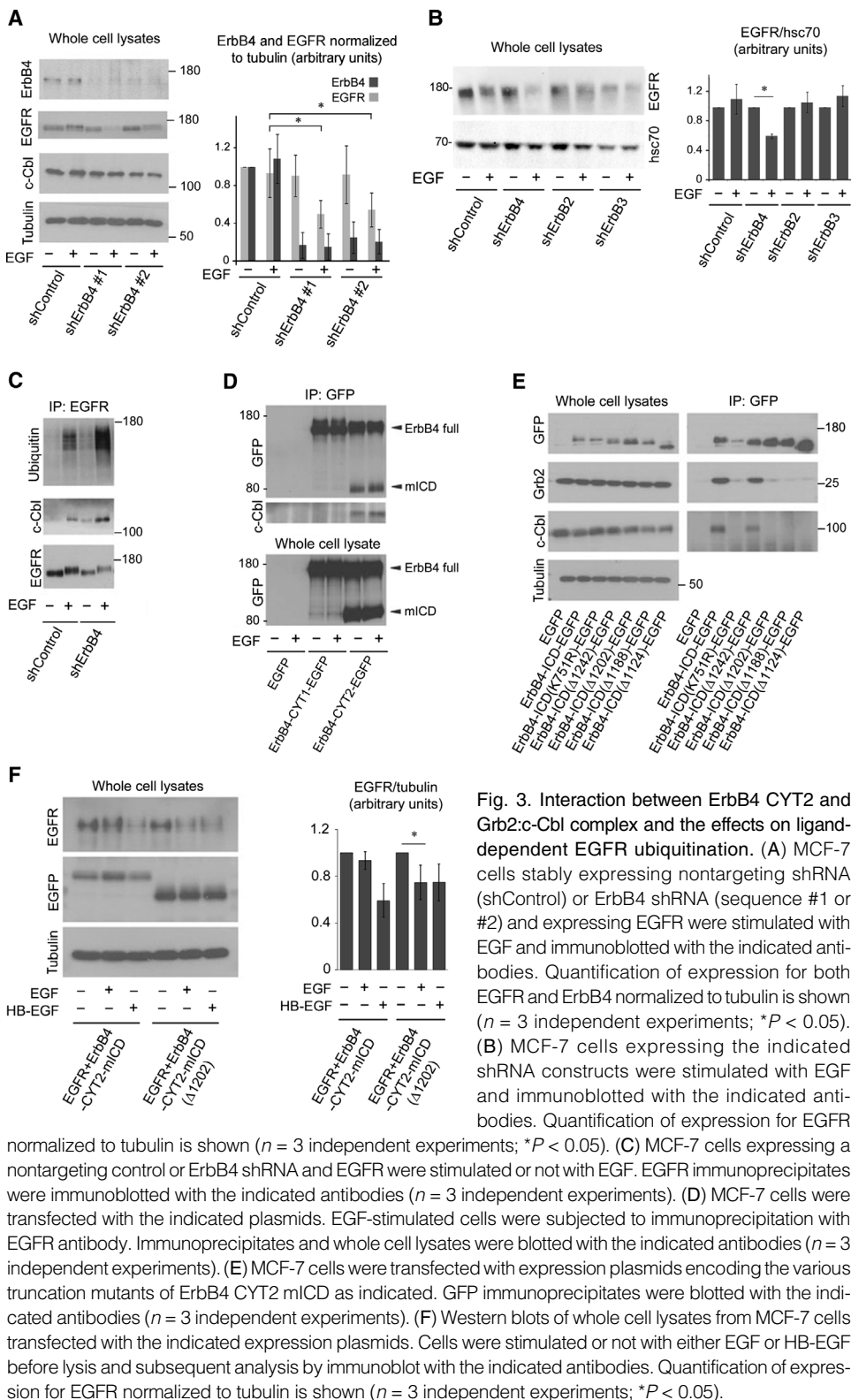


Fig. 3. Interaction between ErbB4 CYT2 and Grb2:c-Cbl complex and the effects on ligand-dependent EGFR ubiquitination. (A) MCF-7 cells stably expressing nontargeting shRNA (shControl) or ErbB4 shRNA (sequence #1 or #2) and expressing EGFR were stimulated with EGF and immunoblotted with the indicated antibodies. Quantification of expression for both EGFR and ErbB4 normalized to tubulin is shown ($n = 3$ independent experiments; $*P < 0.05$). (B) MCF-7 cells expressing the indicated shRNA constructs were stimulated with EGF and immunoblotted with the indicated antibodies. Quantification of expression for EGFR

normalized to tubulin is shown ($n = 3$ independent experiments; $*P < 0.05$). (C) MCF-7 cells expressing a nontargeting control or ErbB4 shRNA and EGFR were stimulated or not with EGF. EGFR immunoprecipitates were immunoblotted with the indicated antibodies ($n = 3$ independent experiments). (D) MCF-7 cells were transfected with the indicated plasmids. EGF-stimulated cells were subjected to immunoprecipitation with EGFR antibody. Immunoprecipitates and whole cell lysates were blotted with the indicated antibodies ($n = 3$ independent experiments). (E) MCF-7 cells were transfected with expression plasmids encoding the various truncation mutants of ErbB4 CYT2 mICD as indicated. GFP immunoprecipitates were blotted with the indicated antibodies ($n = 3$ independent experiments). (F) Western blots of whole cell lysates from MCF-7 cells transfected with the indicated expression plasmids. Cells were stimulated or not with either EGF or HB-EGF before lysis and subsequent analysis by immunoblot with the indicated antibodies. Quantification of expression for EGFR normalized to tubulin is shown ($n = 3$ independent experiments; $*P < 0.05$).

Effect of ErbB4 CYT2 overexpression on EGFR-dependent cell migration

Because Cbl ubiquitin ligase activity correlates with mammary epithelial cell migration (44), we tested the effect of ErbB4 CYT2 mICD expression (which would be expected to sequester c-Cbl) on EGFR-driven cell migration. We performed time-lapse microscopy of MCF-7 cells in the Dunn direct-viewing chemotaxis chamber (45) containing gradients of either EGF or HB-EGF, two EGFR ligands that promote migration in various cell types. Endogenous EGFR is low in abundance in MCF-7 cells, and when exposed to a gradient of either EGF or HB-EGF, these cells did not migrate in the chemotaxis chamber (Fig. 4, A and B). However, after microinjection and overexpression of EGFR, MCF-7 cells migrated in response to either EGF or HB-EGF, as indicated by an increase in cell speed (Fig. 4, A and B), peripheral membrane ruffling, and the extension of lamellipodia (Fig. 4C and movie S1). Although microinjection and expression of ErbB4 CYT2 mICD alone did not affect MCF-7 cell migration (Fig. 4, A and B, and movie S2), cells microinjected with both EGFR and ErbB4 CYT2 mICD migrated significantly faster than cells microinjected with EGFR alone in response to stimulation with either EGF or HB-EGF (Fig. 4, A to C, and movies S3 and S4). Collectively, these findings demonstrate that coexpression of ErbB4 CYT2 with EGFR in MCF-7 cells enhances EGFR-driven cell migration through an increase in cell motility.

Although both EGF and HB-EGF promoted migration in MCF-7 cells overexpressing EGFR and ErbB4 CYT2 mICD, the directional response induced by the growth factor gradient was more pronounced for HB-EGF as shown by the clustering of cell trajectories in the direction of increasing ligand concentration (Fig. 4B). Analysis of the forward migration index (FMI), which provides a measure of chemotaxis (46), confirmed that the directional response of these cells to HB-EGF was significantly greater than the directional response to EGF (Fig. 4B). These data demonstrate that, in our cell system, although EGF and HB-EGF have similar chemokinetic effects and enhance motility to similar extents, HB-EGF is the more effective chemoattractant.

Mutational analysis of the EGFR:ErbB4 CYT2 heterodimer

The current models for intracellular EGFR homodimerization suggest the formation of an asymmetric dimer between the C-terminal

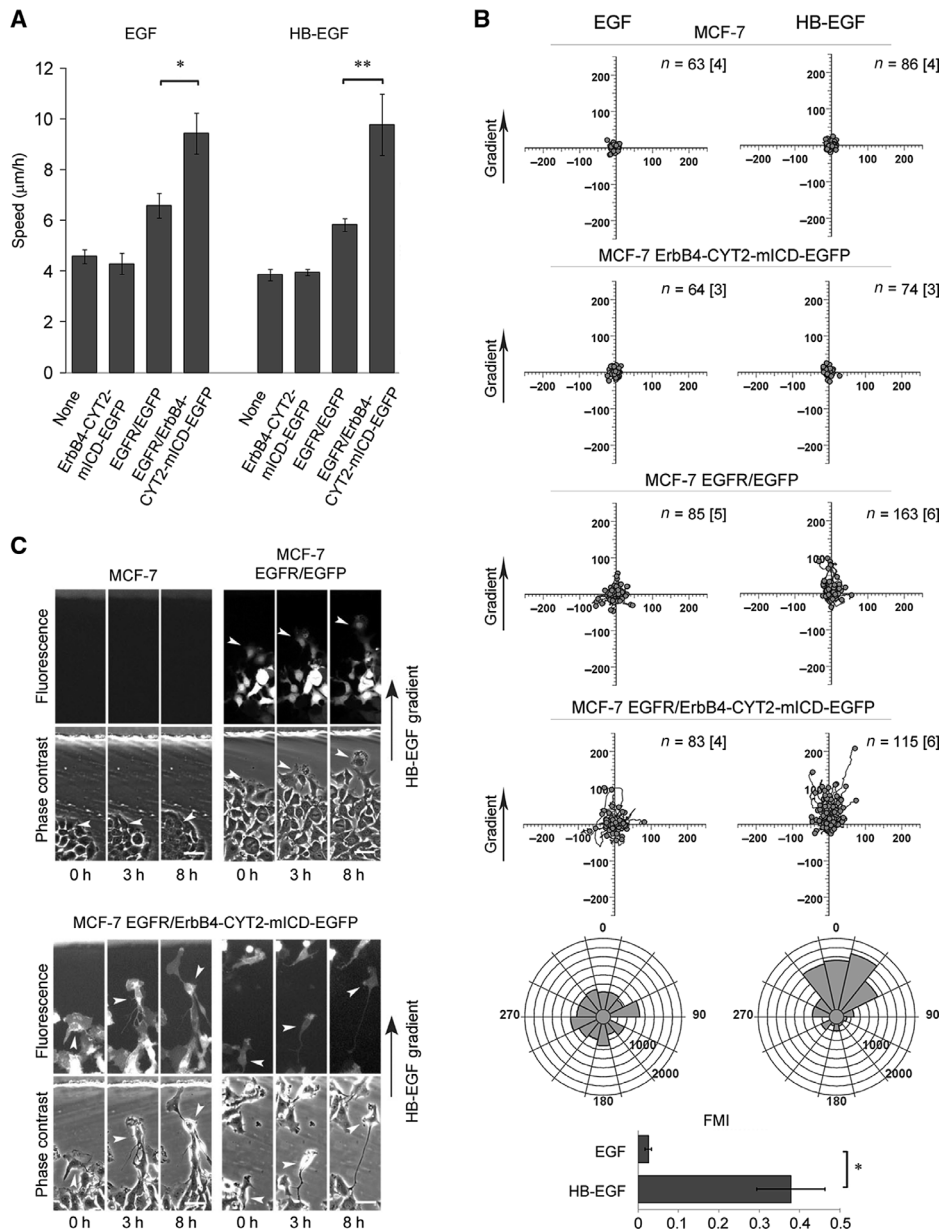


Fig. 4. The effects of ErbB4 CYT2 mICD on EGFR-dependent cell migration. (A) Summary of the speed of migration of MCF-7 cells in response to gradients of either EGF or HB-EGF in the Dunn chemotaxis chamber after microinjection and coexpression of the indicated plasmid combinations ($*P < 0.05$; $**P < 0.01$, two-tailed, unpaired *t* test). Bars represent the mean of means of cell migration speeds from at least 63 cell trajectories obtained from three to six independent experiments. Error bars represent SEM. (B) Track plots summarizing migration data from pooled Dunn chamber chemotaxis assays where MCF-7 cells were either untreated or microinjected with the indicated plasmid combinations and exposed to a gradient of either EGF or HB-EGF as indicated. Arrows indicate the direction of increasing growth factor concentration with respect to each plot. Axes are in micrometers. *n* indicates the total number of cell tracks analyzed for each experimental group, with the number of independent experiments indicated in square brackets. Circular histograms summarize the chemotactic response of cells expressing EGFR and ErbB4 CYT2 mICD in response to gradients of either EGF or HB-EGF. The bar chart summarizes the FMI values calculated for these cells in response to each respective growth factor ($*P < 0.05$). (C) Corresponding fluorescence and phase-contrast image sequences from chemotaxis experiments demonstrating the behavior of MCF-7 cells in an HB-EGF gradient after microinjection and expression of the indicated plasmids. White arrowheads track the position of the cell body over consecutive frames. Scale bar, 50 μm .

lobe of one kinase domain (which acts as the activator) and the N-terminal lobe of another (which acts as the receiver) (47–49). In addition to the kinase domain dimer interface, the JM region also plays a critical role in EGFR phosphorylation through asymmetric dimer formation (50–52). The critical amino acid residue in the JM region is mutated (V689R) in some human cancers (53). The high percentage of sequence identity (79%; fig. S5A) between EGFR and ErbB4 in the relevant regions led us to predict that mutation of the putative interface residues may disrupt the EGFR:ErbB4 dimer. To test this hypothesis, we mutated the EGFR protein only in the JM region (V689R) (which induces partial loss of receiver function), or in combination with a second mutation in the N-terminal lobe (V689R, I706Q) (which induces complete loss of receiver function), or N-terminal lobe plus C-terminal lobe (I706Q, V948R) (which induces loss of both activator and receiver function mutant) (Fig. 5A and fig. S5B).

EGFR phosphorylation was reduced by the combination of the JM mutation (V689R) and a second mutation in the N-terminal lobe (I706Q), or N-terminal lobe (I706Q) plus C-terminal lobe (V948R) (Fig. 5B), but not the JM mutation (V689R) alone. In agreement with these functional results, these combinations of mutations increased the k_{off} for the dimer, indicating that they resulted in destabilized dimers (Fig. 5C). FRET experiments using FLIM revealed decreased interaction between ErbB4 CYT2 and EGFR with the JM (V689R) and N-terminal lobe (I706Q) mutations or with the C-terminal lobe (V948R) and N-terminal lobe (I706Q) mutations (Fig. 5, D and E). Global analysis of fluorescence lifetime data (54, 55) was used to derive the proportion (fractional intensity) of donor fluorophore-labeled ErbB4 that interacted with acceptor-labeled EGFR (wild type or the dimerization mutants). Less of the ErbB4 CYT2 isoform interacted with mutant EGFR than with wild-type EGFR (Fig. 5F). The increase in k_{off} for the EGFR dimerization mutants (as determined from our SPT data) (Fig. 5C), multiplied by a decrease in the fraction of ErbB4 (as assessed by fractional intensity) bound to these EGFR mutants (as measured by ensemble FRET/FLIM), translated to decreased phosphorylation of mutant EGFR (Fig. 5B). These data confirm the involvement of the JM, N, and C lobes in the heterodimer formation between EGFR and ErbB4, as is the case for asymmetric EGFR homodimer.

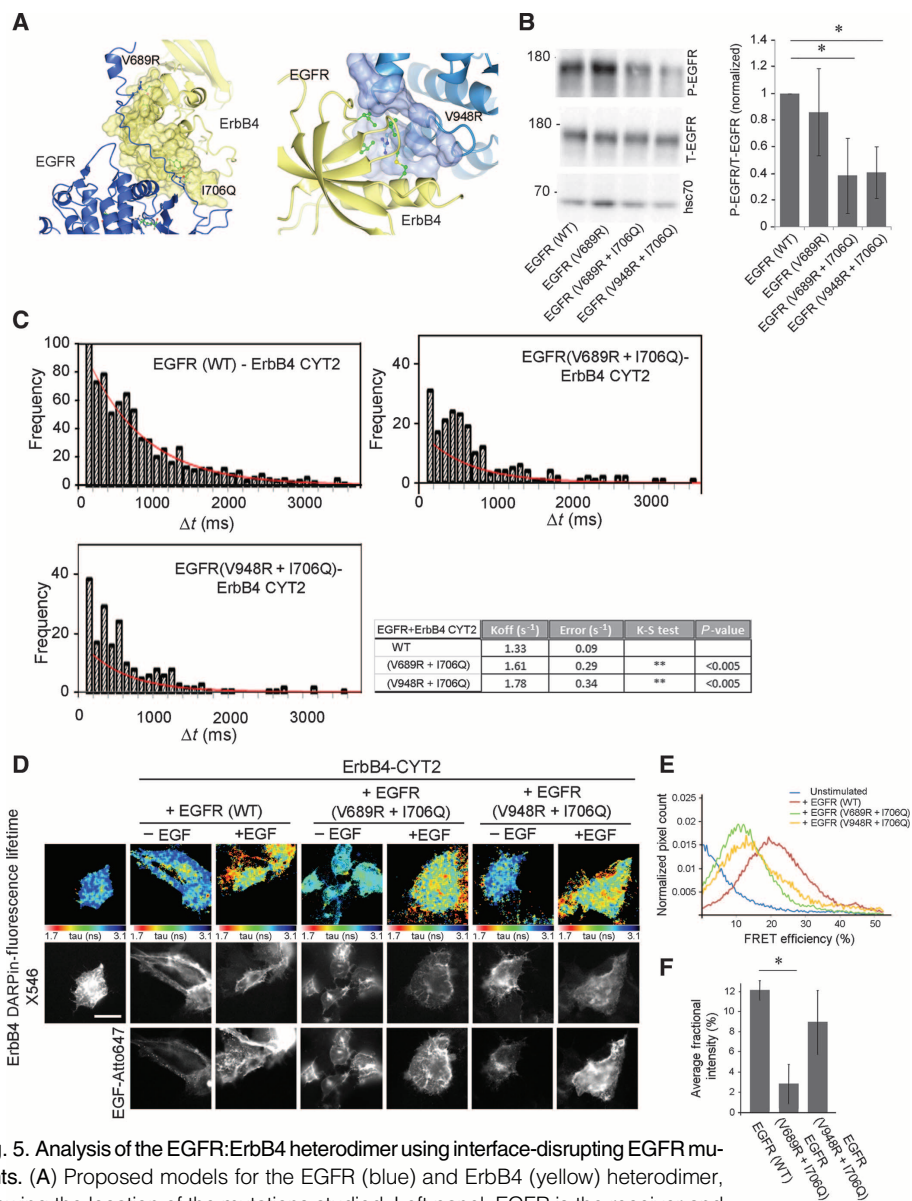


Fig. 5. Analysis of the EGFR:ErbB4 heterodimer using interface-disrupting EGFR mutants. (A) Proposed models for the EGFR (blue) and ErbB4 (yellow) heterodimer, showing the location of the mutations studied. Left panel: EGFR is the receiver and ErbB4 the activator. Right panel: ErbB4 is the receiver and EGFR the activator. The contact surface of the activator molecule is also shown, with the latch of the receiver molecule crossing in front. (B) MCF-7 cells were transfected with the indicated plasmids and stimulated with EGF. Cell lysates were blotted with antibodies as shown. Quantification of phosphorylated EGFR/normalized total EGFR is shown ($n = 3$ independent experiments; $*P < 0.05$). Error bars indicate SD. (C) Single-molecule tracking to determine the dissociation constant of EGFR dimerization mutants with ErbB4 CYT2. Live cells were subsequently incubated with EGF-Atto 647N and anti-ErbB4 DARPIn conjugated to Alexa 546. Graphs show the distribution of the indicated heterodimer lifetimes in cells for all accumulated data ($n = 2$ independent experiments per experimental group; the distribution of more than 2000 dimerization events was fitted to a monoexponential). The difference between wild type (WT) and mutant variants of EGFR in their respective rates of dissociation from ErbB4 (k_{off} values) was significant according to the Kolmogorov-Smirnov test (see table and P values). (D) Spatial distribution of WT EGFR and the indicated mutants with ErbB4 CYT2, using FLIM-based FRET measurements. Transfected MCF-7 cells were stimulated with EGF-Atto 647N before fixation and staining with anti-ErbB4 DARPIn conjugated to Alexa 546. Scale bar, 20 μ m. Lifetime images are presented in a blue-to-red pseudocolor scale, with red indicating short lifetime ($n = 2$ independent experiments per experimental group). (E) FRET efficiency histograms. (F) Bar graphs showing the average fractional intensity of interacting ErbB4 under each experimental condition. Each column represents the mean of 8 to 12 cells per condition ($*P < 0.05$). Error bars indicate SD.

Effect of ErbB4 dimerization–impaired EGFR mutants on cell migration

Next, we examined the migratory function of the ErbB4 dimerization–impaired EGFR mutants. Time-lapse microscopy revealed that migration in response to HB-EGF was impaired in cells expressing either the EGFR (V689R, I706Q) mutant (complete loss of receiver function) or the EGFR (I706Q, V948R) mutant (loss of activator and receiver function) when compared to cells expressing wild-type EGFR (Fig. 6, A and B). Cells expressing wild-type EGFR exhibited chemotaxis toward HB-EGF as demonstrated by the clustering of cell trajectories (Fig. 6B, upper plots) and mean cell directions (Fig. 6B, lower histograms) in the direction of increasing growth factor concentration. The speed of migration of cells expressing the dimerization-impaired mutants, however, was significantly reduced compared to that of wild-type EGFR controls (Fig. 6A), and little to no translocation over the course of time-lapse experiments was observed for these cells (Fig. 6C).

ErbB4 CYT2–dependent switch-like behavior of active EGFR as predicted from a kinetic model of EGFR–ErbB4–Grb2–c-Cbl interactions

To gain a better quantitative understanding of the EGFR–ErbB4 CYT2–c-Cbl interaction network, we constructed a simplified kinetic model of this network focusing on EGFR activation and degradation, which depend on the EGFR interaction with the CYT2 isoform of ErbB4 upon EGF stimulation (text S1). We used the model to interrogate the effect of competing protein-protein interactions in the EGFR–ErbB4 CYT2 network. In particular, we investigated whether competing protein-protein interactions would generate a “switch”-like EGFR response that is dependent on the abundance of the ErbB4 CYT2 isoform.

Our simulations suggest that a gradual increase in the ErbB4 CYT2 concentration leads to a switch-like change in EGFR concentration and activation within a wide range of kinetic constants (fig. S6). As the ErbB4 CYT2 concentration gradually increases, the steady-state amount of total EGFR is initially low but switches to a substantially higher amount when ErbB4 CYT2 concentration exceeds a threshold amount. To assess whether the predicted switches are robust with regard to change in kinetic parameter values, we carried out model

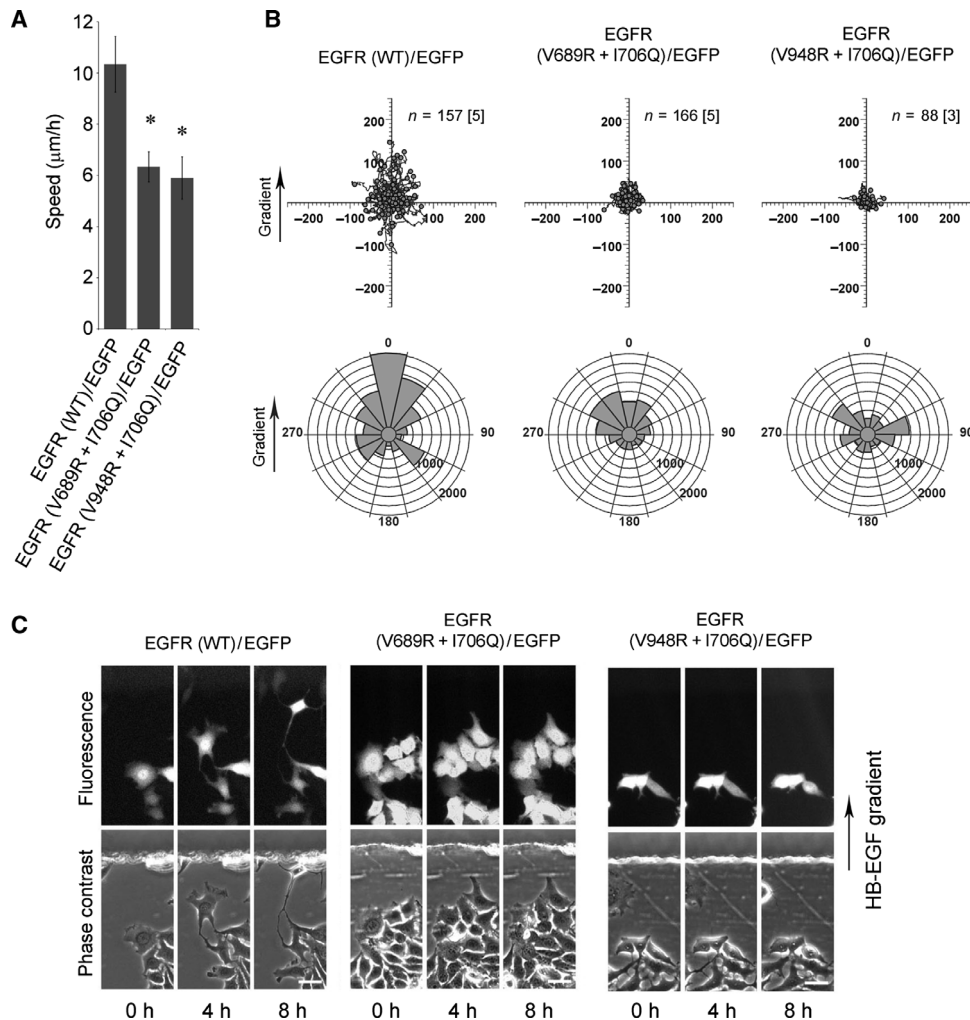


Fig. 6. The effect of mutations that disrupt the EGFR:ErbB4 interface on HB-EGF-stimulated cell migration. (A) Bar graph summarizing the speed of migration of MCF-7 cells in response to gradients of HB-EGF in the Dunn chemotaxis chamber after microinjection and coexpression of the indicated plasmids ($*P < 0.05$, two-tailed, unpaired t test). Bars represent the mean of means of cell migration speeds from at least 88 cell trajectories obtained from three to five independent experiments. Error bars represent SEM. (B) Track plots and circular histograms summarizing the HB-EGF-stimulated migration of MCF-7 cells in the Dunn chamber after the microinjection and coexpression of the indicated plasmids. n indicates the total number of cell tracks analyzed for each experimental group with the number of independent experiments indicated in square brackets. (C) Corresponding fluorescence and phase-contrast image sequences from chemotaxis experiments demonstrating the behavior of MCF-7 cells in an HB-EGF gradient after microinjection and expression of the indicated plasmids. Scale bar, 50 μm .

simulations over multiple random parameter sets (fig. S7). The switch-like behavior of steady-state nondegraded EGFR concentration persists within the entire range, although the switching threshold depends on parameter variations. Model analysis thus suggests that the switch-like protective behavior of the EGFR:ErbB4 CYT2 association controlled by their relative abundances is an intrinsic property of the EGFR-ErbB4-Grb2-c-Cbl interaction network.

DISCUSSION

In the literature, ErbB2 is regarded as the preferred heterodimerization partner of all ErbB partners, and ErbB2 tyrosine kinase activity is required for

neuregulin 2 β (an ErbB4 agonist) to stimulate cell proliferation (51, 56). Here, our ErbB2-4 knockdown experiment that looks for an ErbB that can stabilize EGFR (Fig. 3B) led us to demonstrate the formation of another ErbB heterodimer (EGFR:ErbB4) in breast cancer cell lines. The ErbB4 CYT2 isoform was the major ErbB4 species that contributed to EGFR:ErbB4 heterodimerization and protected EGFR after EGF-induced receptor down-regulation. Mechanistically, the difference between the two ErbB4 isoforms may be due to the lower amount of ErbB4 CYT1 mICD (when compared to that of CYT2 mICD), which is produced after TACE cleavage of ErbB4 and is subjected to greater ubiquitination and degradation by NEDD4 and NEDD4-like E3 ubiquitin protein ligases (27, 41). Furthermore, in the 32D cell system, a hematopoietic cell line devoid of any endogenous ErbB receptors, ErbB4 JMa CYT1, but not JMa CYT2, is localized to intracellular vesicles (57). We also saw a similar although less striking difference in MCF-7 cells. In addition, in the ErbB4 CYT2 variant-expressing cells, the interacting EGFR:ErbB4 CYT2 complex appeared at and around the plasma membrane (Fig. 1A). Together, these suggest that the preference of EGFR to homodimerize with the ErbB4 CYT2 isoform over the ErbB4 CYT1 isoform may in part also be due to the different localization patterns of the two ErbB4 isoforms. By obtaining the kinetic data through live cell SPT-based techniques, quantitative information on dimer affinity was fed into a systems model (fig. S6) that takes into account the genetic and non-genetic sources of variability in protein abundance of the signaling network, to understand the complexity and heterogeneity both in experimental systems and in human disease.

Although there is much systems-level knowledge about the ErbB network (58–61), there is still no obvious strategy of stratifying patients with non-lung tumor types that do not harbor drug-sensitizing mutations for treatment. As a result, EGFR inhibitors tested in various cancer trials have response rates of the order of only 5 to 15% (4, 5). Given the complexity of the ErbB network, the lack of a sustainable effect of ErbB targeting therapies is perhaps not surprising. Furthermore, most of existing systems models of the ErbB network to date have been validated by bulk or ensemble cell biochemistry techniques (62). We coupled ensemble FLIM to global analysis techniques to determine the proportion of ErbB4 molecules undergoing heterodimerization with EGFR at a single-cell level. This stoichiometric information obtained from single cells was further complemented by single-molecule kinetic parameters, derived from live cell SPT. These techniques provide higher-resolution data that may be beneficial

for a better understanding of the complexity and heterogeneity of the ErbB pathways, both in experimental systems and in human disease. The single-molecule resolution is important for assessing the effect of a particular somatic mutation on a specific interacting receptor pair (for example, EGFR and ErbB4) because EGFR can form hetero-oligomers with other ErbB family members and non-ErbB receptors such as c-Met (63), which may act as an intermediary protein within the oligomer. That is, by ensemble/bulk biochemical methods, the effect of mutations may not be detectable or lost through intermediary interactions within a hetero-oligomer.

The ability of the ErbB4 CYT2 isoform (not CYT1) to protect EGFR from degradation can be attributed to binding of c-Cbl to a fragment within the ErbB4 CYT2 mICD (Fig. 3, D to F). The ErbB4 CYT2 isoform (and not other ErbB proteins) sequesters the c-Cbl pool available for interaction with EGFR. Regulation of the efficient recruitment of the Cbl:Grb2 complex to EGFR is a key event for activating threshold-controlled ubiquitination (17) and the subsequent endocytosis of ubiquitinated receptor, which is then committed to lysosomal degradation (15, 16). Our finding that ErbB4 CYT2 (within an EGFR:ErbB4 protein complex) suppresses ligand-induced EGFR down-regulation by sequestering the Cbl:Grb2 component away from its interacting partner (EGFR) reveals an important component of the ErbB network design. This mechanism is likely to amplify or prolong EGFR signaling by increasing the steady-state amount of EGFR. EGFR degradation would then depend on the ErbB4 CYT2 concentration, as well as the dimer competency (conformation) of the respective binding partners (EGFR and ErbB4), in a particular cancer cell. In support of this idea, a core kinetic model of the EGF–EGFR–ErbB4–c-Cbl interactions predicts a switch-like behavior of the steady-state EGFR concentration in response to a graded increase in ErbB4 CYT2 concentration. Our proposed model predicts that the presence of ErbB4 JMa CYT2, together with the availability or propensity of Cbl to bind to EGFR, will determine the steady-state concentration of EGFR, which will in turn dictate the efficacy of ligands (fig. S6). This model is consistent with a previous study reporting that ligand-independent cell survival and breast cancer cell proliferation are enhanced by overexpression of ErbB4 JMa CYT2 but not of the JMa CYT1 isoform (57). An alternative way of regulating the system is by modifying the propensity of Cbl to bind to EGFR. Phosphorylation of EGFR at Tyr¹⁰⁴⁵, which promotes EGFR:Cbl coupling (64), is greater after stimulation with EGF than with amphiregulin (65). At a saturating concentration of EGF, overexpression of the Y1045F EGFR mutant, which is impaired in its ability to bind to Cbl, increases the efficacy of EGF, but not that of amphiregulin, to stimulate cell proliferation. Such disparity of behavior with respect to the two types of ligands is also consistent with our current model.

In breast cancer [in particular, of the basal-like subtype (8)], EGFR abundance is substantially higher in the tumor than in control tissues. However, the prognostic meaning of increased ErbB4 abundance in breast cancer, and in human tumors in general, is less clear. Increased ErbB4 abundance associates with ER positivity and lower tumor grade (66, 67). Conversely, Lodge *et al.* (68) have reported that poor prognostic outcome is associated with increased ErbB4 abundance in node-positive breast cancer patients. Although differences in the patient groups and methodologies used in the scoring of ErbB4 positivity may in part account for differences between these studies, it is likely that the prognostic relevance of increased ErbB4 abundance in breast cancer is further confounded by the complexity of ErbB4 splice variant–dependent signaling. Simply determining the overall abundance of the ErbB4 receptor alone may be insufficient as a reliable determinant of prognostic outcome, because variations in the distribution of different ErbB4 variants may have a substantial impact on the biology of the disease. We showed that variation in the expression of the CYT2 variant largely accounted for the overall differences in *ErbB4* expression observed across tumor samples. Further clinical studies will be needed to analyze

whether the relative expression of the *ErbB4* CYT2 isoform may be a predictive biomarker for assessing the response to EGFR/HER2-targeted therapies, such as lapatinib, among EGFR/HER2 normal breast cancer patients who will benefit from these molecule-targeted agents (9, 10).

We also determined that the ability of the ErbB4 CYT2 variant to promote migration depends on the stability of the EGFR:ErbB4 dimer. Our molecular model for the EGFR:ErbB4 CYT2 heterodimer accurately predicted the interface residues, which when mutated would destabilize the dimer. We compared the k_{off} for the wild-type ErbB4 dimer to those of the EGFR mutants designed on the basis of the model (Fig. 5C). These EGFR mutations destabilized the complex according to our single molecule–based k_{off} determinations in live cells, hence confirming our molecular model. The destabilization of the EGFR:ErbB4 complex, then, abrogates the growth factor–stimulated migration. These data therefore provide mechanistic insight for how the EGFR:ErbB4 CYT2 variant can affect the invasive spread of breast cancer. HB-EGF, but not EGF, induced persistent and directional cell movement (chemotaxis) despite the similar chemokinetic effects of these ligands on EGFR/EGFP- and EGFR/ErbB4 CYT2 mICD–expressing cells. Although HB-EGF stimulation resulted in the rapid down-regulation of EGFR in our experimental system, the chemotactic response toward this ligand was sustained over a period of hours. Therefore, high EGFR concentrations may only be required to initiate migration, whereas a smaller pool of recycling receptors may serve to sustain this behavior over time. We postulate that the trafficking machinery responsible for receptor internalization and subsequent recycling and degradation is essential for maintaining a persistent directional response by establishing a small pool of recycling receptors at the leading edge of polarized cells, as shown previously (69, 70). Although an excessive pool of active receptor may facilitate the rapid mobilization of the motile machinery required for cells to acquire a migratory phenotype, if this pool is sustained over time it will likely impede the cell's ability to localize and therefore polarize this motile machinery and consequently impede persistent directional movement. HB-EGF drives the autonomous metastasis of MDA-MB-231 breast carcinoma cells in vivo, bypassing the need for tumor-associated macrophages to prime tumor cells for invasion (71). Finally, the effect of this alternatively spliced ErbB4 variant on cell motility, through receptor heterodimerization and protection against ubiquitination, means that this variant could be a therapeutic target.

MATERIALS AND METHODS

Reagents and antibodies

EGF and HB-EGF were purchased from PeproTech and Sigma, respectively. All antibodies were purchased from commercial sources: EGFR (sc-120, Santa Cruz Biotechnology Inc.; for immunoprecipitation and for Western blot); ErbB2, ErbB3, ErbB4, c-Cbl, and ubiquitin (Cell Signaling Technology); GFP (Invitrogen); tubulin (Millipore); and hsc70 (Santa Cruz Biotechnology).

Plasmid construction

The plasmid encoding nontagged EGFR was provided by A. Reynolds (Tumor Angiogenesis Group, The Breakthrough Breast Cancer Research Centre, London). Plasmid for C-terminally EGFP206K-tagged EGFR was constructed by inserting EGFR complementary DNA (cDNA) into the pEGFP-N3 vector (Clontech) with the replacement of Ala²⁰⁶ of EGFP by Lys. Plasmid for C-terminally HA-tagged ErbB4 was constructed by inserting ErbB4 cDNA containing a HA epitope tag into the pEGFP-N1 vector (Clontech). ErbB4 CYT2 truncation mutants (including the mICD comprising amino acids 632 to 1292, which represents the membrane-tethered intracellular product of TACE cleavage) were constructed by inserting

polymerase chain reaction–amplified cDNA fragments of ErbB4 into the pEGFP206K-N1 vector. The initial sequence homology search for the identification of putative c-Cbl/Grb2 binding sites was performed using the ErbB4 CYT1 amino acid sequence, and tyrosine residue numbering is therefore based on this sequence (fig. S4). The corresponding residues encoded by the CYT2 ErbB4-mICD, ErbB4-mICD(Δ 1242), ErbB4-mICD(Δ 1202), ErbB4-mICD(Δ 1188), and ErbB4-mICD(Δ 1124) constructs are 632 to 1292, 632 to 1225, 632 to 1185, 632 to 1171, and 632 to 1107, respectively. ErbB4-mICD (K751R) was created by site-directed mutagenesis. cDNAs encoding human ErbB4 CYT1 and CYT2 were described previously (22, 57).

Cell culture, lentivirus-mediated shRNA gene knockdown, and plasmid transfection

MCF-7 and T47D cells were cultured in Dulbecco's modified Eagle's medium supplemented with 10% fetal calf serum. For stable knockdown cell lines, cells were transduced using the Expression Arrest GIPZ lentiviral shRNAmir system (Open Biosystems). The following shRNA oligo IDs from Open Biosystems were used: ErbB4 shRNA #1 (V3LMM 431565), ErbB4 shRNA #2 (V3KMM 431561) for ErbB4 knockdown, and nonsilencing shRNA (RHS4346) for control. Cells were transfected with plasmids using FuGENE6 (Roche) and cultured for 24 hours before experiments. For experiments requiring growth factor stimulation, serum-starved cells were treated with EGF or HB-EGF (100 ng/ml).

Immunoprecipitation and immunoblot analysis

Cells were lysed in lysis buffer [50 mM tris-HCl (pH 7.4), 150 mM NaCl, 1 mM EDTA, 1 mM EGTA, 10% glycerol, 1% Triton X-100, 10 mM NaF, 1 mM Na_3VO_4 , 10 mM *N*-ethylmaleimide, 0.01 μM calyculin A] with Protease Inhibitor Cocktail Set I (Calbiochem). After centrifugation, the supernatants were incubated overnight at 4°C with anti-EGFR or anti-GFP, and subsequently for an additional hour with protein A/G–agarose beads (Alpha Diagnostic International Inc.). After centrifugation, the immunoprecipitates were washed and subjected to SDS–polyacrylamide gel electrophoresis and analyzed by immunoblotting. In cases where quantification of immunoblots is reported, images were processed in ImageJ. Briefly, protein bands from background-subtracted images were normalized to that of their corresponding loading controls (tubulin/hsc70) using the integrated density function. A one-tailed, one-sample *t* test was performed on standardized data ($\mu = 1$) obtained from at least three independent experiments to illustrate the differences between treatment groups. All error bars for graphs summarizing standardized intensity data represent SDs. Statistical tests were performed using the R software package.

Single-molecule imaging of the dissociation rate of the EGFR:ErbB4 complex in live cells

Cells were seeded onto borosilicate glass-bottomed dishes at an appropriate number to reach about 60 to 70% confluence within 24 hours. Then, the sample was serum-deprived through incubation with Opti-MEM (Gibco) for 2 hours at 37°C under 5% CO_2 . Cells were incubated with about 300 pM of Atto 647N–EGF and the anti-ErbB4 DARPin B4_01 (42) equipped with a C-terminal unique cysteine and conjugated to maleimide Alexa 546 for 5 min before imaging. All measurements in live cells were carried out in buffered Opti-MEM in air, and care was taken to ensure a stable pH of the medium for the entire duration of the measurements.

Single-molecule total internal reflection fluorescence microscopy

Single-molecule images were acquired using an objective-type (60 \times , oil, numerical aperture = 1.49; Nikon) total internal reflection setup based on a Nikon Ti Eclipse microscope. Two continuous-wave diode-pumped solid-

state lasers [DTL313 and Stradus (Laser2000)] with emission at 527 and 640 nm, respectively, were used as the excitation source. A combination of lenses and mirrors was used to maximize the excitation light delivered to the microscope and to control the beam size and overlay of the two laser spots. The fluorescence collected through the objective was spectrally split for two-color imaging by passing it through a slit, a dichroic mirror (Semrock FF 665-Di02), and two band-pass filters (Bright Line 692/40, Bright Line 575/25) when using Atto 647N, Alexa 546, or a spectrally similar pair of dyes. Fluorescence was reimaged with an achromatic double lens onto an Evolve electron multiplying charge-coupled device (EMCCD) camera (Photometrics). Images were recorded at a rate of 100 ms/frame.

Single-molecule data analysis

Multicolor single-molecule detection and tracking was performed using the algorithms previously described (72, 73). Channel registration was performed using a cubic polynomial transformation between the channels. Individual molecules were detected using a single-channel feature detection algorithm by comparing two models for the region of interest (ROI) around each pixel. One model assumed that the image region around a pixel is described by pure noise, H_0 (background parameter B_0). Alternatively, when a molecule was present, the image region around a pixel was described by a feature profile from a single point emitter within the pixel plus background emission and stochastic noise, H_1 (background parameter B_1 , feature intensity I , feature coordinates x and y). Given a specific description for each pixel of the background emission, stochastic noise, and feature profile, the probabilities for each of the models in each pixel were calculated using Bayes' theorem, a process known as Bayesian segmentation. Here, the feature profile given by the point spread function of the microscope has been approximated by a Gaussian profile with a fixed, known width. The ROI considered around each pixel was a square with a side size of about four times the assumed feature profile's full width at half-maximum intensity.

Fluorescence intensity time traces were generated using single proximity tracking. A detected feature, i , detected in the first frame was seeding the subsequent frames for which a connection probability that feature i belongs to track j was calculated. Features were assigned to tracks with at most one feature per track and one track per feature based on the above calculated probabilities. Features that were not assigned to existing tracks seeded new tracks starting from the frame in which they were first detected. With the assumption that features are more likely to be linked to tracks in the closest spatial and temporal proximity, this method generates a set of tracks, each of which corresponds to a time series of the detected molecule parameters (intensity, x and y localization). Some tracks may exhibit missing frames because of blinking or nondetected features. A simple method allows following tracks through such gaps. The position coordinates of each detected feature were determined with subpixel resolution by fitting the image of each molecule to a two-dimensional Gaussian function.

The extracted tracks were analyzed for temporal coincidence using custom software in LabVIEW (National Instruments). A homodimer was identified when the feature detected in one channel was persistently located within 1 pixel (160 nm) from a feature in the second channel. The separation distance between the two monomers detected in the green and red channels, respectively [calculated as the Euclidian distance between the (x, y) coordinates of the feature detected in the green and red channels at the same time point t], was plotted as a function of time. To improve the signal-to-noise ratio in separation distance between molecules and, by implication, more accurately determine the duration of a dimerization event, a five-point moving average smoothing filter (10 frames/s) was applied. Additionally, tracks with more than four consecutive frames in which a molecule was not detected were not included in the analysis because the motion of the molecules is unknown in such gaps. Gaps of fewer than four time points

allowed for the fluorophore blinking while enabling us to pick up on the same molecule as it reappeared at the same location. The event duration was measured in a similar way as previously reported (74). Dimer dissociation was marked by a transition in separation distance beyond the threshold value of 1 pixel. The average duration of the dimerization event, τ_{dimer} , was determined by fitting an exponential decay to the histogram of dimer association times using a Marquardt minimization algorithm. The monoexponential function was defined as $f(t) = Z + Ae^{-t/\tau_{\text{dimer}}}$, where Z is a baseline offset and A is the amplitude of the exponential function. Fitting was performed with the baseline offset constraint to be positive. The dissociation rate k_{off} was determined as $1/\tau_{\text{dimer}}$ with the error $\Delta k_{\text{off}} = \Delta \tau_{\text{dimer}}/\tau_{\text{dimer}}^2$.

FRET determination by FLIM measurements

Processing of cells for FRET determination by FLIM has been previously described (70). FLIM was performed using time-correlated single-photon counting (TCSPC) with a multiphoton microscope system as described previously (75). The fractional intensity of the interacting species was calculated as previously described (54, 55). A two-tailed, unpaired t test was used to illustrate differences in the average fractional intensities observed between treatment groups.

Microinjection

Cells were seeded at a density of 1×10^5 on 20 mm \times 20 mm No. 1 borosilicate coverslips in normal growth medium and cultured for 48 hours before microinjection. For microinjection, medium was supplemented with 25 mM Hepes. Microinjection was performed using a FemtoJet microinjector (Eppendorf) in conjunction with an Eppendorf 5171 micro-manipulator mounted on a Zeiss Axio35 inverted microscope using pre-pulled FemtoTipII microinjection capillaries (Eppendorf). Plasmids were reconstituted to a final concentration of 50 ng/ml each in microinjection buffer (1:1 phosphate-buffered saline/H₂O) and centrifuged at 13,000 rpm for 15 min before microcapillary loading. Plasmid constructs were microinjected into the cytoplasm of cells rather than the nucleus to minimize insult to the cells and to allow more time for recovery as expression is delayed until the next cell division cycle. After microinjection, cells were washed three times with normal growth medium and cultured for an additional 24 hours before commencement of chemotaxis assays. A diamond pen was used to score a semicircular etch on the underside of coverslips before cell seeding to aid in the positioning of microinjected cells within the diffusion gap of the chemotaxis chamber.

Evaluation of chemotaxis and statistical analysis of cell behavior

Evaluation of chemotaxis was performed using the Dunn Direct-Viewing Chemotaxis chamber (45) in conjunction with automated digital time-lapse microscopy essentially as described previously (76). Dunn chambers were purchased from Hawksley Scientific, and a detailed description of the chamber and its assembly can be found elsewhere (77, 78). Time-lapse imaging of microinjected cells within the diffusion gap of the chemotaxis chamber was performed using an Olympus IX71 inverted wide-field microscope fitted with an automated xy stage (Ludl), automated shutters, excitation and emission filter wheels (Ludl), CCD camera (Andor), and halogen and mercury lamps for phase-contrast and epifluorescence imaging, respectively. Andor iQ image acquisition software was used for the automated control of the microscope and peripheral devices during time-lapse experiments. The automated xy stage enables the imaging of multiple fields across multiple chemotaxis chambers over the course of time-lapse experiments, and the entire body of the microscope was housed within an environment chamber stably maintained at 37°C. For time-lapse experiments, sequential phase-contrast and epifluorescence images were

acquired every 10 min for a duration of 16 hours to record the behavior of microinjected cells in the gradient. Post-acquisition tracking and analysis of cell behavior was performed using purpose-written software developed in-house. Briefly, interactive tracking of cells over the course of time-lapse film sequences was used to generate individual cell trajectories for the analysis of cell speed and directionality. Cell trajectories were used to generate track plots and circular histograms for the visual representation of migration data. Track plots represent pooled cell trajectories, shifted to a common origin, for all cells from a given treatment group. Circular histograms were used for the graphical representation of chemotaxis. For each histogram, the size of a segment represents the percentage of cells whose mean direction of migration lies within that data bin multiplied by the mean speed of migration for all cells of that data bin. For all histograms, 0° represents migration directly toward the outer well of the Dunn chamber. The FMI was used for the evaluation of directionality (46, 76, 79). A two-tailed, two-sample t test was used to test the significance of differences in cell speed between treatment groups. The exact Mann-Whitney U test was used to test the significance of differences in directionality. Statistical tests were performed using the R software package. Detailed methods for the evaluation of directionality from cell trajectory data have been described previously (76).

Exon array analysis of ErbB4 variants in human breast cancers

The transcriptional abundances of ErbB4 and its variants were determined from the analysis of Human Exon 1.0 ST Array (Affymetrix) data on breast cancer samples (80). On the basis of immunohistochemistry-derived quantification of ER and HER2, together with RNA and DNA expression inferred from microarray data, 155 samples were consistently classified as ER⁺ HER2⁻ ($n = 16$), ER⁻ HER2⁺ ($n = 19$), and ER⁻ HER2⁻ ($n = 120$). Data were processed using the Aroma Affymetrix R framework (<http://www.aroma-project.org/>), and individual exon and overall transcript abundances were computed. Variant specific scores were calculated as follows: Score(CYT1) = $\log[\text{Intensity}(\text{CYT1})] - \log[\text{Intensity}(\text{CYT1} + \text{CYT2})] + C1$; Score(CYT2) = $\log[\text{Intensity}(\text{CYT1} + \text{CYT2})] - \log[\text{Intensity}(\text{CYT1})] + C2$. The constants $C1$ and $C2$ are chosen to make the minimum of the scores equal to zero. Variant scores provide an indication of the relative contribution of the two variants to the overall *ERBB4* gene transcription, across different tumor groups. Global trends of the abundance of CYT1 and CYT2 across tumor groups were also confirmed by FIRMA-based analyses (81).

Modeling the EGFR:ErbB4 dimer interface

The EGFR-ErbB4 and ErbB4-EGFR computer models were created using a combination of Coot (82) and VMD (83). The figure was prepared using CCP4mg (84).

SUPPLEMENTARY MATERIALS

www.sciencesignaling.org/cgi/content/full/7/339/ra78/DC1

- Text S1. Development of a core model of the EGFR-ErbB4 CYT2 interaction network.
 Fig. S1. Evaluation of the subcellular localization of tagged ErbB4 isoforms by immunofluorescence.
 Fig. S2. Abundance of *ErbB4* exon-specific sequences in 404 human breast cancer samples within the TCGA RNASeq database.
 Fig. S3. The effect of knockdown of individual ErbB family members on EGF-dependent EGFR degradation.
 Fig. S4. Schematic of conserved and putative c-Cbl and Grb2 binding sites in ErbB4 JMA CYT1.
 Fig. S5. Sequence homology alignment of the EGFR and ErbB4 CYT2 dimerization domains and associated residues targeted for mutagenesis.
 Fig. S6. Kinetic model of the core EGFR:ErbB4 CYT2 interaction network.
 Fig. S7. Simulated steady-state concentrations of total EGFR over random parameter sets.

Table S1. Reactions and reaction rates of the core EGFR–ErbB4 CYT2 interaction model.
 Table S2. Ordinary differential equations of the core EGFR–ErbB4 CYT2 interaction model.
 Movie S1. Migration of EGFR- and EGFP-expressing MCF-7 cells in an HB-EGF gradient.
 Movie S2. Migration of ErbB4 CYT2 mCD–EGFP–expressing MCF-7 cells in an HB-EGF gradient.
 Movies S3 and S4. Two examples of EGFR- and ErbB4 CYT2–expressing MCF-7 cells chemotaxing toward an HB-EGF gradient.
 References (85–88)

REFERENCES AND NOTES

1. A. Citri, Y. Yarden, EGF-ERBB signalling: Towards the systems level. *Nat. Rev. Mol. Cell Biol.* **7**, 505–516 (2006).
2. Y. Yarden, M. X. Sliwkowski, Untangling the ErbB signalling network. *Nat. Rev. Mol. Cell Biol.* **2**, 127–137 (2001).
3. M. Fukuoka, S. Yano, G. Giaccone, T. Tamura, K. Nakagawa, J. Y. Douillard, Y. Nishiwaki, J. Vansteenkiste, S. Kudoh, D. Rischin, R. Eek, T. Horai, K. Noda, I. Takata, E. Smit, S. Averbuch, A. Macleod, A. Feyereislova, R. P. Dong, J. Baselga, Multi-institutional randomized phase II trial of gefitinib for previously treated patients with advanced non–small-cell lung cancer (The IDEAL 1 Trial) [corrected]. *J. Clin. Oncol.* **21**, 2237–2246 (2003).
4. E. E. Cohen, F. Rosen, W. M. Stadler, W. Recant, K. Stenson, D. Huo, E. E. Vokes, Phase II trial of ZD1839 in recurrent or metastatic squamous cell carcinoma of the head and neck. *J. Clin. Oncol.* **21**, 1980–1987 (2003).
5. L. B. Saltz, N. J. Meropol, P. J. Loehrer Sr., M. N. Needle, J. Kopit, R. J. Mayer, Phase II trial of cetuximab in patients with refractory colorectal cancer that expresses the epidermal growth factor receptor. *J. Clin. Oncol.* **22**, 1201–1208 (2004).
6. R. Perez-Soler, A. Chachoua, L. A. Hammond, E. K. Rowinsky, M. Huberman, D. Karp, J. Rigas, G. M. Clark, P. Santabarbara, P. Bonomi, Determinants of tumor response and survival with erlotinib in patients with non–small-cell lung cancer. *J. Clin. Oncol.* **22**, 3238–3247 (2004).
7. A. F. Leary, S. Drury, S. Detre, S. Pancholi, A. E. Lykkesfeldt, L. A. Martin, M. Dowsett, S. R. D. Johnston, Lapatinib restores hormone sensitivity with differential effects on estrogen receptor signaling in cell models of human epidermal growth factor receptor 2–negative breast cancer with acquired endocrine resistance. *Clin. Cancer Res.* **16**, 1486–1497 (2010).
8. C. A. Hudis, L. Gianni, Triple-negative breast cancer: An unmet medical need. *Oncologist* **16** (Suppl. 1), 1–11 (2011).
9. A. Evans, A. F. Leary, S. R. Johnston, R. A. Her, J. M. Bliss, M. H. Hills, C. Harper-Wynne, N. Bundred, G. Coombes, R. Sahoo, S. Detre, I. E. Smith, M. Dowsett, Lapatinib has antiproliferative effects in both HER2 positive (+) and HER2 negative (–) breast cancer (BC): Results from the MAPLE short-term pre-surgical trial (CRUK E/06/039). *Cancer Res.* **72** (Suppl. 1), abstract LB-222 (2012).
10. I. A. Mayer, C. L. Arteaga, Does lapatinib work against HER2-negative breast cancers? *Clin. Cancer Res.* **16**, 1355–1357 (2010).
11. K. Zhang, J. Sun, N. Liu, D. Wen, D. Chang, A. Thomason, S. K. Yoshinaga, Transformation of NIH 3T3 cells by HER3 or HER4 receptors requires the presence of HER1 or HER2. *J. Biol. Chem.* **271**, 3884–3890 (1996).
12. B. D. Cohen, P. A. Kiener, J. M. Green, L. Foy, H. P. Fell, K. Zhang, The relationship between human epidermal growth-like factor receptor expression and cellular transformation in NIH3T3 cells. *J. Biol. Chem.* **271**, 30897–30903 (1996).
13. D. J. Riese II, D. F. Stern, Specificity within the EGF family/ErbB receptor family signaling network. *Bioessays* **20**, 41–48 (1998).
14. M. A. Alaoui-Jamali, D. J. Song, N. Benlimame, L. Yen, X. Deng, M. Hernandez-Perez, T. Wang, Regulation of multiple tumor microenvironment markers by overexpression of single or paired combinations of ErbB receptors. *Cancer Res.* **63**, 3764–3774 (2003).
15. S. Sigismund, E. Argenzio, D. Tosoni, E. Cavallaro, S. Polo, P. P. Di Fiore, Clathrin-mediated internalization is essential for sustained EGFR signaling but dispensable for degradation. *Dev. Cell* **15**, 209–219 (2008).
16. S. Sigismund, T. Woelk, C. Puri, E. Maspero, C. Tacchetti, P. Transidico, P. P. Di Fiore, S. Polo, Clathrin-independent endocytosis of ubiquitinated cargos. *Proc. Natl. Acad. Sci. U.S.A.* **102**, 2760–2765 (2005).
17. S. Sigismund, V. Algisi, G. Nappo, A. Conte, R. Pascolutti, A. Cuomo, T. Bonaldi, E. Argenzio, L. G. Verhoef, E. Maspero, F. Bianchi, F. Capuani, A. Ciliberto, S. Polo, P. P. Di Fiore, Threshold-controlled ubiquitination of the EGFR directs receptor fate. *EMBO J.* **32**, 2140–2157 (2013).
18. G. Levkowitz, H. Waterman, S. A. Ettenberg, M. Katz, A. Y. Tsygankov, I. Alroy, S. Lavi, K. Iwai, Y. Reiss, A. Ciechanover, S. Lipkowitz, Y. Yarden, Ubiquitin ligase activity and tyrosine phosphorylation underlie suppression of growth factor signaling by c-Cbl/Sli-1. *Mol. Cell* **4**, 1029–1040 (1999).
19. J. J. Tao, P. Castel, N. Radosevic-Robin, M. Elkabets, N. Auricchio, N. Aceto, G. Weitsman, P. Barber, B. Vojnovic, H. Ellis, N. Morse, N. T. Viola-Villegas, A. Bosch, D. Juric, S. Hazra, S. Singh, P. Kim, A. Bergamaschi, S. Maheswaran, T. Ng, F. Penault-Llorca, J. S. Lewis, L. A. Carey, C. M. Perou, J. Baselga, M. Scaltriti, Antagonism of EGFR and HER3 enhances the response to inhibitors of the PI3K-Akt pathway in triple-negative breast cancer. *Sci. Signal.* **7**, ra29 (2014).
20. C. M. Perou, T. Sørlie, M. B. Eisen, M. van de Rijn, S. S. Jeffrey, C. A. Rees, J. R. Pollack, D. T. Ross, H. Johnsen, L. A. Akslen, O. Fluge, A. Pergamenschikov, C. Williams, S. X. Zhu, P. E. Lanning, A. L. Børresen-Dale, P. O. Brown, D. Botstein, Molecular portraits of human breast tumours. *Nature* **406**, 747–752 (2000).
21. M. Sundvall, K. Iljin, S. Kilpinen, H. Sara, O. P. Kallioniemi, K. Elenius, Role of ErbB4 in breast cancer. *J. Mammary Gland Biol. Neoplasia* **13**, 259–268 (2008).
22. K. Elenius, C. J. Choi, S. Paul, E. Santiestevan, E. Nishi, M. Klagsbrun, Characterization of a naturally occurring ErbB4 isoform that does not bind or activate phosphatidylinositol 3-kinase. *Oncogene* **18**, 2607–2615 (1999).
23. V. Kainulainen, M. Sundvall, J. A. Määttä, E. Santiestevan, M. Klagsbrun, K. Elenius, A natural ErbB4 isoform that does not activate phosphoinositide 3-kinase mediates proliferation but not survival or chemotaxis. *J. Biol. Chem.* **275**, 8641–8649 (2000).
24. J. Omerovic, L. Santangelo, E. M. Puggioni, J. Marrocco, C. Dall'Armi, C. Palumbo, F. Belleudi, L. Di Marcotullio, L. Frati, M. R. Torrisi, G. Cesareni, A. Gulino, M. Alimandi, The E3 ligase Aip4/Ich ubiquitinates and targets ErbB-4 for degradation. *FASEB J.* **21**, 2849–2862 (2007).
25. M. Sundvall, A. Korhonen, I. Paatero, E. Gaudio, G. Melino, C. M. Croce, R. I. Aqilan, K. Elenius, Isoform-specific monoubiquitination, endocytosis, and degradation of alternatively spliced ErbB4 isoforms. *Proc. Natl. Acad. Sci. U.S.A.* **105**, 4162–4167 (2008).
26. F. Y. Feng, S. Varambally, S. A. Tomlins, P. Y. Chun, C. A. Lopez, X. Li, M. A. Davis, A. M. Chinnaiyan, T. S. Lawrence, M. K. Nyati, Role of epidermal growth factor receptor degradation in gemcitabine-mediated cytotoxicity. *Oncogene* **26**, 3431–3439 (2007).
27. F. Zeng, J. Xu, R. C. Harris, Nedd4 mediates ErbB4 JM-a/CYT-1 ICD ubiquitination and degradation in MDCK II cells. *FASEB J.* **23**, 1935–1945 (2009).
28. T. T. Junttila, M. Sundvall, M. Lundin, J. Lundin, M. Tanner, P. Härkönen, H. Joensuu, J. Isola, K. Elenius, Cleavable ErbB4 isoform in estrogen receptor–regulated growth of breast cancer cells. *Cancer Res.* **65**, 1384–1393 (2005).
29. N. Anilkumar, M. Parsons, R. Monk, T. Ng, J. C. Adams, Interaction of fascin and protein kinase C α : A novel intersection in cell adhesion and motility. *EMBO J.* **22**, 5390–5402 (2003).
30. J. W. Legg, C. A. Lewis, M. Parsons, T. Ng, C. M. Isacke, A novel PKC-regulated mechanism controls CD44–ezrin association and directional cell motility. *Nat. Cell Biol.* **4**, 399–407 (2002).
31. T. Ng, M. Parsons, W. E. Hughes, J. Monypenny, D. Zicha, A. Gautreau, M. Arpin, S. Gschmeissner, P. J. Verveer, P. I. Bastiaens, P. J. Parker, Ezrin is a downstream effector of trafficking PKC–integrin complexes involved in the control of cell motility. *EMBO J.* **20**, 2723–2741 (2001).
32. T. Ng, A. Squire, G. Hansra, F. Bomancin, C. Prevostel, A. Hanby, W. Harris, D. Barnes, S. Schmidt, H. Mellor, P. I. Bastiaens, P. J. Parker, Imaging protein kinase C α activation in cells. *Science* **283**, 2085–2089 (1999).
33. M. Parsons, M. D. Keppler, A. Kline, A. Messent, M. J. Humphries, R. Gilchrist, I. R. Hart, C. Quittau-Prevostel, W. E. Hughes, P. J. Parker, T. Ng, Site-directed perturbation of protein kinase C–integrin interaction blocks carcinoma cell chemotaxis. *Mol. Cell Biol.* **22**, 5897–5911 (2002).
34. M. Parsons, J. Monypenny, S. M. Ameer-Beg, T. H. Millard, L. M. Machesky, M. Peter, M. D. Keppler, G. Schiavo, R. Watson, J. Chernoff, D. Zicha, B. Vojnovic, T. Ng, Spatially distinct binding of Cdc42 to PAK1 and N-WASP in breast carcinoma cells. *Mol. Cell Biol.* **25**, 1680–1695 (2005).
35. S. Prag, M. Parsons, M. D. Keppler, S. M. Ameer-Beg, P. Barber, J. Hunt, A. J. Beavil, R. Calvert, M. Arpin, B. Vojnovic, T. Ng, Activated ezrin promotes cell migration through recruitment of the GEF Dbl to lipid rafts and preferential downstream activation of Cdc42. *Mol. Biol. Cell* **18**, 2935–2948 (2007).
36. G. Tarcic, S. K. Boguslavsky, J. Wakim, T. Kiuchi, A. Liu, F. Reinitz, D. Nathanson, T. Takahashi, P. S. Mischel, T. Ng, Y. Yarden, An unbiased screen identifies DEP-1 tumor suppressor as a phosphatase controlling EGFR endocytosis. *Curr. Biol.* **19**, 1788–1798 (2009).
37. E. M. Bublil, G. Pines, G. Patel, G. Fruhwirth, T. Ng, Y. Yarden, Kinase-mediated quasi-dimers of EGFR. *FASEB J.* **24**, 4744–4755 (2010).
38. R. Iwamoto, E. Mekada, Heparin-binding EGF-like growth factor: A juxtacrine growth factor. *Cytokine Growth Factor Rev.* **11**, 335–344 (2000).
39. C. Y. Ni, M. P. Murphy, T. E. Golde, G. Carpenter, γ -Secretase cleavage and nuclear localization of ErbB-4 receptor tyrosine kinase. *Science* **294**, 2179–2181 (2001).
40. M. Hatakeyama, N. Yumoto, X. Yu, M. Shirouzu, S. Yokoyama, A. Konagaya, Transformation potency of ErbB heterodimer signaling is determined by B-Raf kinase. *Oncogene* **23**, 5023–5031 (2004).
41. Y. Li, Z. Zhou, M. Alimandi, C. Chen, WW domain containing E3 ubiquitin protein ligase 1 targets the full-length ErbB4 for ubiquitin-mediated degradation in breast cancer. *Oncogene* **28**, 2948–2958 (2009).
42. D. Steiner, P. Forrer, A. Plückthun, Efficient selection of DARPins with sub-nanomolar affinities using SRP phage display. *J. Mol. Biol.* **382**, 1211–1227 (2008).

43. A. Sorkin, L. K. Goh, Endocytosis and intracellular trafficking of ErbBs. *Exp. Cell Res.* **314**, 3093–3106 (2008).
44. L. Duan, S. M. Raja, G. Chen, S. Virmani, S. H. Williams, R. J. Clubb, C. Mukhopadhyay, M. A. Rainey, G. Ying, M. Dimri, J. Chen, A. L. Reddi, M. Naramura, V. Band, H. Band, Negative regulation of EGFR-Vav2 signaling axis by Cbl ubiquitin ligase controls EGF receptor-mediated epithelial cell adherens junction dynamics and cell migration. *J. Biol. Chem.* **286**, 620–633 (2011).
45. D. Zicha, G. A. Dunn, A. F. Brown, A new direct-viewing chemotaxis chamber. *J. Cell Sci.* **99**, 769–775 (1991).
46. E. F. Foxman, E. J. Kunkel, E. C. Butcher, Integrating conflicting chemotactic signals. The role of memory in leukocyte navigation. *J. Cell Biol.* **147**, 577–588 (1999).
47. X. Zhang, J. Gureasko, K. Shen, P. A. Cole, J. Kuriyan, An allosteric mechanism for activation of the kinase domain of epidermal growth factor receptor. *Cell* **125**, 1137–1149 (2006).
48. X. Zhang, K. A. Pickin, R. Bose, N. Jura, P. A. Cole, J. Kuriyan, Inhibition of the EGF receptor by binding of MIG6 to an activating kinase domain interface. *Nature* **450**, 741–744 (2007).
49. H. Zhang, A. Berezov, Q. Wang, G. Zhang, J. Drebin, R. Murali, M. I. Greene, ErbB receptors: From oncogenes to targeted cancer therapies. *J. Clin. Invest.* **117**, 2051–2058 (2007).
50. S. T. Low-Nam, K. A. Lidke, P. J. Cutler, R. C. Roovers, P. M. van Bergen en Henegouwen, B. S. Wilson, D. S. Lidke, ErbB1 dimerization is promoted by domain co-confinement and stabilized by ligand binding. *Nat. Struct. Mol. Biol.* **18**, 1244–1249 (2011).
51. D. Graus-Porta, R. R. Beerli, J. M. Daly, N. E. Hynes, ErbB-2, the preferred heterodimerization partner of all ErbB receptors, is a mediator of lateral signaling. *EMBO J.* **16**, 1647–1655 (1997).
52. K. Aertgeerts, R. Skene, J. Yano, B. C. Sang, H. Zou, G. Snell, A. Jennings, K. Iwamoto, N. Habuka, A. Hirokawa, T. Ishikawa, T. Tanaka, H. Miki, Y. Ohta, S. Sogabe, Structural analysis of the mechanism of inhibition and allosteric activation of the kinase domain of HER2 protein. *J. Biol. Chem.* **286**, 18756–18765 (2011).
53. T. Y. Chou, C. H. Chiu, L. H. Li, C. Y. Hsiao, C. Y. Tzen, K. T. Chang, Y. M. Chen, R. P. Peng, S. F. Tsai, C. M. Tsai, Mutation in the tyrosine kinase domain of epidermal growth factor receptor is a predictive and prognostic factor for gefitinib treatment in patients with non-small cell lung cancer. *Clin. Cancer Res.* **11**, 3750–3757 (2005).
54. P. R. Barber, S. M. Ameer-Beg, J. Gilbey, L. M. Carlin, M. Keppler, T. C. Ng, B. Vojnovic, Multiphoton time-domain fluorescence lifetime imaging microscopy: Practical application to protein-protein interactions using global analysis. *J. R. Soc. Interface* **6**, S93–S105 (2009).
55. K. Makrogianneli, L. M. Carlin, M. D. Keppler, D. R. Matthews, E. Ofo, A. Coolen, S. M. Ameer-Beg, P. R. Barber, B. Vojnovic, T. Ng, Integrating receptor signal inputs that influence small Rho GTPase activation dynamics at the immunological synapse. *Mol. Cell Biol.* **29**, 2997–3006 (2009).
56. C. P. Mill, M. D. Zordan, S. M. Rothenberg, J. Settleman, J. F. Leary, D. J. Riese II, ErbB2 is necessary for ErbB4 ligands to stimulate oncogenic activities in models of human breast. *Cancer Genes Cancer* **2**, 792–804 (2011).
57. J. A. Määttä, M. Sundvall, T. T. Junttila, L. Peri, V. J. Laine, J. Isola, M. Egeblad, K. Elenius, Proteolytic cleavage and phosphorylation of a tumor-associated ErbB4 isoform promote ligand-independent survival and cancer cell growth. *Mol. Biol. Cell* **17**, 67–79 (2006).
58. H. S. Wiley, S. Y. Shvartsman, D. A. Lauffenburger, Computational modeling of the EGF-receptor system: A paradigm for systems biology. *Trends Cell Biol.* **13**, 43–50 (2003).
59. B. S. Hendriks, J. Cook, J. M. Burke, J. M. Beusmans, D. A. Lauffenburger, D. de Graaf, Computational modelling of ErbB family phosphorylation dynamics in response to transforming growth factor alpha and heregulin indicates spatial compartmentation of phosphatase activity. *Syst. Biol.* **153**, 22–33 (2006).
60. B. N. Kholodenko, O. V. Demin, G. Moehren, J. B. Hoek, Quantification of short term signaling by the epidermal growth factor receptor. *J. Biol. Chem.* **274**, 30169–30181 (1999).
61. H. Shankaran, H. S. Wiley, H. Resat, Modeling the effects of HER/ErbB1-3 coexpression on receptor dimerization and biological response. *Biophys. J.* **90**, 3993–4009 (2006).
62. M. F. Ciaccio, J. P. Wagner, C. P. Chuu, D. A. Lauffenburger, R. B. Jones, Systems analysis of EGF receptor signaling dynamics with microwestern arrays. *Nat. Methods* **7**, 148–155 (2010).
63. A. Z. Lai, J. V. Abella, M. Park, Crosstalk in Met receptor oncogenesis. *Trends Cell Biol.* **19**, 542–551 (2009).
64. L. M. Grøvdal, E. Stang, A. Sorkin, I. H. Madhus, Direct interaction of Cbl with pTyr 1045 of the EGF receptor (EGFR) is required to sort the EGFR to lysosomes for degradation. *Exp. Cell Res.* **300**, 388–395 (2004).
65. K. J. Wilson, C. Mill, S. Lambert, J. Buchman, T. R. Wilson, V. Hernandez-Gordillo, R. M. Gallo, L. M. Ades, J. Settleman, D. J. Riese II, EGFR ligands exhibit functional differences in models of paracrine and autocrine signaling. *Growth Factors* **30**, 107–116 (2012).
66. V. Pawlowski, F. Révillion, M. Hebban, L. Hornez, J. P. Peyrat, Prognostic value of the type I growth factor receptors in a large series of human primary breast cancers quantified with a real-time reverse transcription-polymerase chain reaction assay. *Clin. Cancer Res.* **6**, 4217–4225 (2000).
67. C. J. Witton, J. R. Reeves, J. J. Goings, T. G. Cooke, J. M. Bartlett, Expression of the HER1–4 family of receptor tyrosine kinases in breast cancer. *J. Pathol.* **200**, 290–297 (2003).
68. A. J. Lodge, J. J. Anderson, W. J. Gullick, B. Haugk, R. C. F. Leonard, B. Angus, Type 1 growth factor receptor expression in node positive breast cancer: Adverse prognostic significance of c-erbB-4. *J. Clin. Pathol.* **56**, 300–304 (2003).
69. M. Bailly, J. Wyckoff, B. Bouzahzah, R. Hammerman, V. Sylvestre, M. Cammer, R. Pestell, J. E. Segall, Epidermal growth factor receptor distribution during chemotactic responses. *Mol. Biol. Cell* **11**, 3873–3883 (2000).
70. M. Parsons, T. Ng, Intracellular coupling of adhesion receptors: Molecular proximity measurements. *Methods Cell Biol.* **69**, 261–278 (2002).
71. Z. N. Zhou, V. P. Sharma, B. T. Beaty, M. Roh-Johnson, E. A. Peterson, N. Van Rooijen, P. A. Kenny, H. S. Wiley, J. S. Condeelis, J. E. Segall, Autocrine HBEGF expression promotes breast cancer intravasation, metastasis and macrophage-independent invasion in vivo. *Oncogene* **33**, 3784–3793 (2014).
72. D. J. Rolfe, C. I. McLachlan, M. Hirsch, S. R. Needham, C. J. Tynan, S. E. Webb, M. L. Martin-Fernandez, M. P. Hobson, Automated multidimensional single molecule fluorescence microscopy feature detection and tracking. *Eur. Biophys. J.* **40**, 1167–1186 (2011).
73. S. E. Webb, S. K. Roberts, S. R. Needham, C. J. Tynan, D. J. Rolfe, M. D. Winn, D. T. Clarke, R. Barraclough, M. L. Martin-Fernandez, Single-molecule imaging and fluorescence lifetime imaging microscopy show different structures for high- and low-affinity epidermal growth factor receptors in A431 cells. *Biophys. J.* **94**, 803–819 (2008).
74. H. P. Lu, L. Xun, X. S. Xie, Single-molecule enzymatic dynamics. *Science* **282**, 1877–1882 (1998).
75. F. Festy, S. M. Ameer-Beg, T. Ng, K. Suhling, Imaging proteins in vivo using fluorescence lifetime microscopy. *Mol. Biosyst.* **3**, 381–391 (2007).
76. J. Monypenny, D. Zicha, C. Higashida, F. Ocegueda-Yanez, S. Narumiya, N. Watanabe, Cdc42 and Rac family GTPases regulate mode and speed but not direction of primary fibroblast migration during platelet-derived growth factor-dependent chemotaxis. *Mol. Cell Biol.* **29**, 2730–2747 (2009).
77. S. E. Webb, J. W. Pollard, G. E. Jones, Direct observation and quantification of macrophage chemoattraction to the growth factor CSF-1. *J. Cell Sci.* **109** (Pt. 4), 793–803 (1996).
78. D. Zicha, G. A. Dunn, Are growth factors chemotactic agents? *Exp. Cell Res.* **221**, 526–529 (1995).
79. H. Zhang, L. Vutskits, V. Calao, P. Durbec, J. Z. Kiss, A role for the polysialic acid-neuronal cell adhesion molecule in PDGF-induced chemotaxis of oligodendrocyte precursor cells. *J. Cell Sci.* **117**, 93–103 (2004).
80. E. de Rinaldis, P. Gazinska, A. Mera, Z. Modrusan, G. M. Fedorowicz, B. Burford, C. Gillett, P. Marra, A. Grigoriadis, D. Dorman, L. Holmberg, S. Pinder, A. Tutt, Integrated genomic analysis of triple-negative breast cancers reveals novel microRNAs associated with clinical and molecular phenotypes and sheds light on the pathways they control. *BMC Genomics* **14**, 643 (2013).
81. E. Purdom, K. M. Simpson, M. D. Robinson, J. G. Conboy, A. V. Lapuk, T. P. Speed, FIRMA: A method for detection of alternative splicing from exon array data. *Bioinformatics* **24**, 1707–1714 (2008).
82. P. Emsley, B. Lohkamp, W. G. Scott, K. Cowtan, Features and development of Coot. *Acta Crystallogr. D Biol. Crystallogr.* **66**, 486–501 (2010).
83. W. Humphrey, A. Dalke, K. Schulten, VMD: Visual molecular dynamics. *J. Mol. Graphics* **14**, 33–38, 27–28 (1996).
84. S. McNicholas, E. Potterton, K. S. Wilson, M. E. Noble, Presenting your structures: The CCP4mg molecular-graphics software. *Acta Crystallogr. D Biol. Crystallogr.* **67**, 386–394 (2011).
85. H. S. Wiley, J. J. Herbst, B. J. Walsh, D. A. Lauffenburger, M. G. Rosenfeld, G. N. Gill, The role of tyrosine kinase activity in endocytosis, compartmentation, and down-regulation of the epidermal growth factor receptor. *J. Biol. Chem.* **266**, 11083–11094 (1991).
86. A. Tomas, C. E. Futter, E. R. Eden, EGF receptor trafficking: Consequences for signaling and cancer. *Trends Cell Biol.* **24**, 26–34 (2014).
87. L. K. Nguyen, M. A. Cavadas, C. C. Scholz, S. F. Fitzpatrick, U. Bruning, E. P. Cummins, M. M. Tambuwala, M. C. Manresa, B. N. Kholodenko, C. T. Taylor, A. Cheong, A dynamic model of the hypoxia-inducible factor 1 α (HIF-1 α) network. *J. Cell Sci.* **126**, 1454–1463 (2013).
88. M. R. Birtwistle, M. Hatakeyama, N. Yumoto, B. A. Ogunnaike, J. B. Hoek, B. N. Kholodenko, Ligand-dependent responses of the ErbB signaling network: Experimental and modeling analyses. *Mol. Syst. Biol.* **3**, 144 (2007).

Acknowledgments: We are grateful to T. Coolen for his expert advice and review of the statistical analyses. **Funding:** This work was supported by KCL Breakthrough Breast Cancer Research Unit funding (T.K., J.M., B.B., E.d.R., and P.M.) that was awarded to A.T., and an endowment fund from Dimpleby Cancer Care to King's College London (S.A.-B. and T.N.). N.W., S.P.P., K.L., and G.F., as well as the FLIM system, were supported

by the KCL-UCL Comprehensive Cancer Imaging Centre (CCIC) funding [CR-UK and EPSRC, in association with the MRC and DoH (England)] (to T.N.). J.B., E.O.-Z., D.R.M., V.D., and O.C. were supported by a BBSRC Programme grant (to P.P. and M.L.M.-F.). L.K.N. and B.N.K. were supported by funding provided by SFI (grant no. 06/CE/B1129) and PRIMES (FP7-HEALTH-2011-278568). **Author contributions:** T.K., E.O.-Z., J.M., J.B., and O.C. performed the experiments and analyzed the results. T.K., P.P., and T.N. designed the research. N.W., S.P., and C.E.G. performed the pathological analyses, and K.L., B.B., D.D., M.A.S., and E.d.R. performed the genomic and associated bioinformatics analyses on the patient samples. G.F., P.M., Y.L.B., A.P., W.J.G., and Y.Y. provided reagents, technical assistance, and conceptual advice. M.W. provided the structural modeling. D.R.M., D.J.R., V.D., S.P.P., M.L.M.-F., and S.A.-B. constructed the custom-made single-molecule imaging platform and associated analysis software, as well as assisted in acquiring the imaging data. G.S. and A.T. provided the clinical input for designing the genomic experiment and the interpretation of data. L.K.N. and B.N.K. performed kinetic modeling analysis. T.K., E.O.-Z., J.M., and T.N. wrote the manuscript. **Competing interests:**

The authors declare that they have no competing interests. **Data and materials availability:** Access to patient tissue samples and data is regulated under the Human Tissue Act and Guy's and St Thomas' Hospital Tissue Bank Access Committee.

Submitted 6 February 2014

Accepted 23 July 2014

Final Publication 19 August 2014

10.1126/scisignal.2005157

Citation: T. Kiuchi, E. Ortiz-Zapater, J. Monypenny, D. R. Matthews, L. K. Nguyen, J. Barbeau, O. Coban, K. Lawler, B. Burford, D. J. Rolfe, E. de Rinaldis, D. Dafou, M. A. Simpson, N. Woodman, S. Pinder, C. E. Gillett, V. Devauges, S. P. Poland, G. Fruhwirth, P. Marra, Y. L. Boersma, A. Plückthun, W. J. Gullick, Y. Yarden, G. Santis, M. Winn, B. N. Kholodenko, M. L. Martin-Fernandez, P. Parker, A. Tutt, S. M. Ameer-Beg, T. Ng, The ErbB4 CYT2 variant protects EGFR from ligand-induced degradation to enhance cancer cell motility. *Sci. Signal.* 7, ra78 (2014).